Single-cell RNA-sequencing implicates venous endothelial cells as a source of VEGF-A-mediated neo-angiogenesis in neuroinflammation

S. Shahriar[1, 2*], S. Biswas[3*], K. Zhao[3], U. Akcan[3], M. C. Tuohy[3], M. D. Glendinning[3], A. Kurt[3], C. R. Wayne[3], G. Prochilo[4], M. Z. Price[4], R. A. Brekken[5], V. Menon[3**] and D. Agalliu[1, 3, 6**]

Departments of [1]Pathology & Cell Biology, [3]Neurology and [4]Biological Sciences, Columbia University Irving Medical Center, New York, NY 10032, USA.

[2]Wyss Institute for Biologically Inspired Engineering, Boston, MA 02115, USA.

[5]Department of Surgery, University of Texas Southwestern Medical Center, Dallas, TX 75390 USA.

*equal contribution first authors

**equal contribution senior authors

[6]Corresponding author: E-mail: da191@cumc.columbia.edu

Mailing address:

Columbia University Irving Medical Center

650 West 168th Street

Black Building Room 310

New York, NY 10032

Telephone: 212-305-0323

ORCID: 0000-0002-5375-4143

ABSTRACT

Histopathological studies of multiple sclerosis (MS), a demyelinating disease of the central nervous system (CNS), and its animal model, experimental autoimmune encephalomyelitis (EAE), have found newly formed leaky vessels in demyelinated acute and chronic plaques, in addition to blood-brain barrier (BBB) damage in existing vessels, that exacerbate disease pathology by increasing infiltration of immune cells. Which vessel subtypes and signaling pathways generate these aberrant vessels is poorly understood. Using single-cell RNA-sequencing and *in vivo* validation, we find that transcriptome signatures of neo-angiogenesis arise in venous endothelial cells in both acute and chronic EAE, and correlate with upregulation in VEGF-A signaling. These neo-angiogenic markers are also increased in acute and chronic MS lesions. Treatment with a VEGF-A blocking antibody diminishes neo-angiogenic transcriptomic signatures and vascular proliferation *in vivo*, but does not restore BBB function or ameliorate significantly EAE pathology. Therefore, anti-angiogenic therapies in combination with immunomodulatory therapies may benefit MS progression.

INTRODUCTION

Multiple sclerosis (MS) is a chronic, autoimmune, inflammatory demyelinating disease of the central nervous system (CNS), in which activated leukocytes invade the CNS to trigger neuroinflammation, demyelination, gliosis, and axonal damage and resection[1,2]. Inflammation of CNS endothelial cells (ECs) associated with focal breakdown of the blood-brain barrier (BBB) is prevalent in demyelinating MS plaques[3]. Abnormalities in BBB tight junctions precede the onset of clinical experimental autoimmune encephalomyelitis (EAE), the animal model for MS, as observed in histological[4-7], MRI[8], and *in vivo* two-photon imaging studies[9]. Endothelial tight junction abnormalities persist throughout the disease course and correlate with clinical severity in both MS[10,11] and EAE[4,5] due to their permissive role in leukocyte migration across the BBB[12-15]. Recent studies have shown that MS-associated single nucleotide polymorphisms are enriched in ECs compared to other CNS cells[16], consistent with a critical role for the CNS endothelium in MS pathogenesis.

Angiogenesis is most active during CNS development in rodents and humans, and is absent in the adult CNS[17]. In addition to BBB damage in existing CNS vessels, neo-angiogenesis (the formation of abnormal new vessels) has been observed surrounding acute and chronic MS plaques[18,19]. Many blood vessels within MS/EAE lesions have an irregular morphology[20], and express proliferation markers[21]. Vessel density is increased in demyelinating lesions during both peak and relapsing EAE, as well as in relapsing-remitting MS (RRMS) and secondary progressive MS (SPMS)[22-26]. A recent 3T SWI-FLAIR imaging study of the brain vasculature in RRMS patients using a 3T SWI-FLAIR also revealed several vascular abnormalities including small lesions at the vessel boundary, dilated vessels and developmental venous angiomas within MS lesions[27]. Most studies suggest that neo-angiogenesis worsens MS/EAE pathogenesis[18,19] since its blockade improves clinical scores and attenuates demyelination and neuroinflammation in EAE[26,28]. However, the timing and relation of neo-angiogenesis to EAE/MS progression, and its molecular characterization, vascular origin, and underlying signaling pathways remain poorly understood.

Vascular endothelial growth factor A (VEGF-A) is a key mediator of angiogenesis in normal vascular development[29], and in pathologies such as cancers[30], ocular conditions[31] and inflammatory diseases. VEGF-A expression is upregulated in acute and chronic MS plaques[20] and EAE[26,28]. Serum VEGF-A levels are significantly higher in relapsing MS, compared to either remitting MS patients, or healthy cases, and correlate with lesion length on MRI examination[20,32]. Bevacizumab (Avastin®) is a recombinant, humanized monoclonal antibody that inhibits VEGF-A by blocking its binding to VEGF Receptor 2 (VEGFR2) and VEGFR1[33-35]. Administration of either bevacizumab, or the monoclonal antibody B20.4-1-1 that binds both murine and human VEGF-A[28], in mice prior to and during EAE induction improves clinical disease and attenuates both demyelination and inflammation[26,28]. VEGF-A modulates also immune cell function and suppresses host immunity in the tumor microenvironment[36]. Critically, previous studies have failed to disentangle whether VEGF-A blockade ameliorates EAE clinical and histopathological outcomes by inhibiting angiogenesis, or by reducing peripheral immune cell activation and CNS infiltration.

85 In addition to VEGF-A signaling, the Wnt/β-catenin pathway is critical for both
86 developmental angiogenesis and BBB formation and maintenance in the healthy CNS[37-41]. We
87 have previously shown that the Wnt/β-catenin pathway is reactivated in CNS ECs during EAE and
88 MS. Its inhibition in CNS ECs in mice prior to EAE onset exacerbates disease outcomes, increases
89 $CD4^+$ T cell infiltration into the CNS, and exacerbates demyelination by increasing expression of
90 Vascular cell adhesion molecule-1 (Vcam1) and Caveolin-1, two proteins critical for lymphocyte
91 attachment and migration across the BBB[9,42]. Whether activation of the Wnt/β-catenin signaling
92 in EAE/MS promotes neo-angiogenesis together with VEGF-A remains unknown.
93
94 To address which vessel subtypes and signaling pathways drive neo-angiogenesis and
95 characterize its molecular signatures in neuroinflammation, we performed single-cell RNA-
96 sequencing (scRNA-seq), and subsequent *in vivo* validation in control, acute and chronic MOG_{35-}
97 $_{55}$ EAE mice. We find that transcriptomic signatures of neo-angiogenesis are upregulated in venous
98 ECs in both acute and chronic EAE, and correlate with upregulation in VEGF-A, but not Wnt/β-
99 catenin, signaling. These neo-angiogenic markers are also increased in acute and chronic MS
100 lesions. Treatment with the VEGF-A blocking antibody r84[43,44] diminishes neo-angiogenic
101 transcriptomic signatures and reduces vascular proliferation *in vivo*, but fails to restore BBB
102 function or significantly ameliorate EAE pathology. Our study provides a comprehensive
103 molecular understanding of the origin and mechanism of neo-angiogenesis in EAE/MS, and
104 suggests that anti-angiogenic therapies in combination with immunomodulatory therapies may
105 benefit MS progression.
106
107
108 **RESULTS**
109 **ECs isolated from spinal cords of control and EAE mice cluster based on A-V zonation and**
110 **disease state**
111 To determine which vessel subtypes and signaling pathways drive neo-angiogenesis in
112 EAE, we induced MOG_{35-55} EAE in 12-week-old *TCF/LEF1::*H2B::eGFP (Wnt reporter) female
113 mice[9,42]. We combined spinal cords from 2 mice for each sample, and collected the tissue at acute
114 peak [score = 2-4; 16-17 days post-immunization (d.p.i.); n=8 mice, 4 samples] and early chronic
115 (score ≤ 1; 28-29 d.p.i.; n=8 mice, 4 samples) disease for scRNA-seq (**Figure 1a**). Age-matched

healthy (n=6 mice, 3 samples) and Complete Freund's Adjuvant (CFA)-immunized mice (n=6 mice, 3 samples) served as controls. Acute and chronic EAE mice had a similar disease course with no difference in disease onset, or peak clinical score. The clinical score on the day of collection was higher in the acute compared to chronic cohort (CFA mice did not have any disease; **Extended Data Figure 1a-e**). Spinal cords were dissociated into single-cell suspensions and Wnt-positive ($eGFP^+$) and Wnt-negative ($eGFP^-$) $CD31^+$ ECs were sorted and pooled for scRNA-seq (**Extended Data Figure 1f**). After quality filtering[45] and *in silico* EC selection based on expression of *Pecam1*, *Cldn5*, and *Erg*[46], we performed graph-based clustering to separate 45,309 ECs collected from from 14 samples [4 acute EAE, 4 chronic EAE, 3 healthy and 3 CFA controls (28 total mice, 2 mice/sample, **Extended Data Table 1-1**)] into distinct clusters based on their transcriptomic expression profiles.

Graph-based clustering at high resolution separated the ECs into 23 distinct clusters, which were visualized using a *t*-distributed stochastic neighbor embedding (t-SNE) representation (**Figure 1c-f)**. While these original 23 clusters are not necessarily functionally distinct, this "overclustering" approach was used to establish clear boundaries among cells belonging to each of the major vessel subtype. Overclustering was followed by remerging clusters defined by computational or biological measures; this two-step process can avoid suboptimal clustering boundaries that often arise when using lower resolution clustering[47]. After the merging step, we assigned a major subtype identity to each EC cluster based on expression of canonical markers for arteries, capillaries and veins[48] (**Figure 1b**). Expression of arterial and venous markers peaked in clusters visualized at opposite ends of the t-SNE plot; putative capillary clusters organized themselves between these ends in t-SNE embedding (**Figure 1e, f**). Although non-local distances in t-SNE plots are highly nonlinear, the overall arrangement of ECs suggests that arteriovenous (AV) zonation was a major putative axis of variation in the EC data (**Figure 1b, e**). The disease state was the second putative axis of variation since ECs purified from acute and chronic EAE formed separate groups from those isolated from controls (**Figure 1c, d, Extended Data Figure 1i**). To validate the robustness of vascular subtype classifications for our single cell clusters, we compared p-value distributions of differentially expressed genes among subtypes from shuffled data where we randomly ordered the cell cluster assignments. The differential gene lists specific to vascular subtype cluster demonstrated substantially and significantly more hits than those

147 obtained from random shuffling, an indication that despite the sparsity and dropouts inherent in
148 of single-cell datasets, the signal retains biological relevance for vascular subtype identification
149 (data not shown). Given that our samples were processed in separate batches (**Extended Data**
150 **Table 1-1**), we conducted clustering with and without Harmony-based[49] batch correction to assess
151 the degree of batch effects (**Extended Data Figure 1g, h**). Comparing cluster membership before
152 and after batch correction revealed insignificant batch impact on the membership of the four major
153 vascular subtypes, signifying the robustness of vascular subtype clustering to batch effects. The
154 minimal influence of batch on subtype clustering is additionally corroborated visually by the
155 overlay of batch structure onto the individual vascular subtype-specific t-SNE plots (**Extended**
156 **Data Figure 1i**). Finally, quantification of *eGFP* mRNA expression within the single-cell dataset
157 revealed that Wnt/β-catenin signaling was highest in capillary ECs (cECs), moderate in arterial
158 ECs (aECs) and venule ECs (vnECs), and low-to-absent in venous ECs (vECs) (**Extended Data**
159 **Fig. 1j**).
160

161 **Transcriptomic signatures of neo-angiogenesis arise in venous ECs in both acute and chronic**
162 **EAE**

163 EC clusters belonging to each vascular subtype (6,856 aECs; 30,208 cECs; 6,596 vnECs,
164 and 1,649 vECs) were subclustered separately and visualized again with t-SNE (**Figure 2a-h**).
165 Arterial ECs from acute EAE formed a separate sub-cluster from chronic EAE and control samples
166 which clustered together (**Figure 2a, b, i, j**), suggesting that transcriptomic changes induced by
167 neuroinflammation are transient in aECs. In contrast, cECs, vnECs, and vECs isolated from
168 control, acute, and chronic EAE formed distinct sub-clusters (**Figure 2c-j**), indicative of more
169 persistent transcriptomic changes during neuroinflammation. The control (healthy and CFA)-
170 enriched cluster in both cEC and vnEC populations contained a higher proportion of ECs
171 originating from chronic versus acute EAE (**Figure 2i, j**). In contrast, the control-enriched cluster
172 in vECs contained only a small percentage of ECs from chronic EAE (**Figure 2i, j**). Overall, the
173 control samples (healthy and CFA) have similar transcriptional profiles, except in vnECs where
174 they cluster separately due to increased expression of inflammatory gene signatures in CFA
175 (**Figure 2e, f, i, j**; data not shown). Lastly, there were no observed differences in the proportions
176 of aECs, cECs, vnECs, and vECs collected from both healthy and diseased samples (**Figure 2j**).

177 These data confirm that ECs undergo transcriptional shifts in both acute and chronic EAE,
178 consistent with prior reports using bulk and scRNA-seq[50,51].
179
180 To identify key transcriptomic signatures driving EC clustering, we performed differential
181 gene expression (DE) analysis comparing the acute- and chronic-EAE to control-enriched EC
182 clusters for each vessel subtype (**Extended Data Table 1-3 to 1-9**). This data was used to conduct
183 gene set enrichment analysis (GSEA)[52] using curated and comprehensive gene catalogs (**Extended**
184 **Data Table 1-2**) for various cellular and molecular pathways and functions from the Molecular
185 Signatures Database v6.1 (*MSigDB: software.broadinstitute.org/gsea/msigdb/genesets.jsp*) and
186 published sources[53,54], and determine which processes were enriched for significantly up- and
187 downregulated genes in diseased ECs from each vessel subtype (**Extended Data Table 1-3 to 1-**
188 **9**).
189
190 Gene sets associated with inflammation, antigen processing and presentation, and
191 chemokine/cytokine signaling were upregulated in all ECs from acute EAE (**Figure 3a**), and those
192 associated with inflammation and antigen processing and presentation were also upregulated in
193 cECs and vECs from chronic EAE (**Figure 3c**). In contrast, expression of the BBB gene set was
194 significantly downregulated in diseased cECs, vnECs, and vECs in both acute and chronic EAE
195 (**Figure 3b, d**), consistent with a dysfunctional BBB[50,51]. Surprisingly, expression of BBB genes
196 was upregulated in acute aECs relative to controls (**Figure 3a**), which may explain the transient
197 nature of neuroinflammatory transcriptomic changes in aECs (**Figure 2b**).
198
199 Angiogenesis involves several steps ranging from tip and stalk EC specification, tip cell-
200 mediated extracellular matrix (ECM) degradation, EC migration and proliferation[55]. Pathological
201 tumor angiogenesis is also regulated, in part, by endothelial-to-mesenchymal transition (EndoMT),
202 which induces delamination of resident ECs and subsequent acquisition of a mesenchymal
203 phenotype with invasive/migratory properties[56,57]. DE analysis of diseased versus control vnECs
204 and vECs revealed that the top-upregulated genes are enriched for angiogenic and tip cell markers
205 (features of neo-angiogenesis) in both acute and chronic EAE (**Figure 3e**; **Extended Data Figure**
206 **2**). Several angiogenesis ("tip cells", "angiogenesis", "EC proliferation" and "EC migration") and
207 angiogenesis-related ("ECM" [58], "EndoMT" [59]) gene signatures were significantly upregulated in

208 diseased veins (acute and chronic) together with two pro-angiogenic pathways ("VEGF" and
209 "TGF-β")[60-62] (**Figure 3a, c**). Acute vnECs also showed upregulation of gene signatures for tip
210 cells in acute EAE (**Figure 3a**). In contrast, arterial or capillary ECs in acute EAE were not
211 enriched for transcriptional gene signatures of neo-angiogenesis compared to controls. In fact,
212 expression of angiogenesis-related gene sets were downregulated in diseased aECs relative to
213 controls, suggesting a vascular repair process and inverse correlation between BBB and
214 angiogenesis-related genes (**Figure 3b**). Although several angiogenesis pathways were
215 upregulated in EAE vECs, the Wnt/β-catenin signaling was almost absent in healthy vECs and
216 downregulated in chronic EAE vECs (**Figure 3d; Extended Data Figure 1j**). In summary, our
217 scRNAseq data reveal that transcriptomic signatures for neo-angiogenesis are upregulated in
218 vECs, and to a lesser extent in vnECs, in acute and chronic EAE. While Wnt/β-catenin signaling
219 is essential for developmental CNS angiogenesis[17], it is likely not associated with pathological
220 neo-angiogenesis in EAE.
221
222 **Congruency analysis reveals a unique transcriptome signature of neuroinflammation-**
223 **related angiogenesis in EAE**
224 We next asked to what extent neuroinflammation-related neo-angiogenesis shares similar
225 transcriptomic signatures with either CNS developmental or tumor angiogenesis. We analyzed
226 publicly available datasets of murine lung tumor Ecs (TECs)[63] and developmental CNS Ecs
227 [DECs; embryonic day 14.5 (E14.5)][64] to identify angiogenic genes that were significantly
228 upregulated in expression during tumor and CNS developmental angiogenesis, respectively.
229 Comparing those gene sets to the angiogenic gene signature of acute EAE vECs revealed that most
230 angiogenic genes in neuroinflammation were also upregulated in developmental (~68%) and tumor
231 (~85%) angiogenesis (**Extended Data Figure 3a-b**). There was a greater number of acute EAE
232 vEC genes shared with TECs than with DECs, suggesting that neuroinflammation angiogenesis is
233 more similar at the molecular level with tumor angiogenesis. We also analyzed the congruency in
234 angiogenic gene expression between DECs and TECs (**Extended Data Figure 3c**). While
235 pathogenic and developmental angiogenic gene signatures had many common genes (105), they
236 also had a significant number of unique genes (DECs had 102 unique genes and TECs had 79),
237 suggesting that the two processes are substantially different. Therefore, neuroinflammation and

238 tumor angiogenesis have a higher congruency at the gene signature level, compared to
239 neurodevelopmental angiogenesis.
240
241 To confirm these computational analyses *in vivo*, we analyzed expression of Apelin (*Apln*),
242 one of the non-congruent angiogenic markers identified through the computational analysis
243 between DECs and EAE vECs, in developing (P3), healthy adult, and acute EAE spinal cord
244 tissues via mRNA *in situ* hybridization (**Extended Data Figure 3d-i**). *Apln* is a positive modulator
245 of angiogenesis and is enriched in proliferating Ecs and tip cells in the P7 brain[65]. *Apln*$^{-/-}$ mouse
246 retinas show delayed EC proliferation, vascular outgrowth and branching[66]. Consistent with prior
247 studies[65], *Apln* mRNA was highly expressed by many developing blood vessels in the P3 spinal
248 cord; however, its expression was abolished in the healthy adult CNS, except in the vasculature of
249 the choroid plexus and meninges, and in some neurons (**Extended Data Figure 3d-i;** data not
250 shown). *Apln* expression was not induced in inflamed blood vessels near white matter lesions of
251 acute EAE spinal cords (**Extended Data Figure 3d-i**), validating that neurodevelopmental and
252 neuroinflammatory angiogenesis are distinct at the transcriptome level.
253
254 **Venous ECs undergo proliferation and express angiogenesis markers in acute and chronic**
255 **EAE**
256 To validate the neo-angiogenic transcriptome signature observed in vECs in EAE (**Figure**
257 **3a, c**), we examined the expression of the proliferation marker Ki67 in arteries, capillaries, and
258 veins in longitudinal (sagittal) spinal cord sections from control (CFA), acute and chronic EAE
259 mice (**Figure 4a**). We used EphB4 as a marker for venous and venular ECs[67-69], and Caveolin-1
260 to label all ECs. Consistent with scRNA-seq data for the *Mki67* transcript (**Figure 4b**), vECs in
261 both acute and chronic EAE spinal cords showed significantly higher proliferation (Ki67^{+} ECs)
262 compared to CFA controls (**Figure 4c, d**). The vascular coverage of EphB4^{+} vECs and venule
263 diameter were increased significantly in acute and chronic EAE compared to the CFA spinal cords
264 (**Figure 4c-f**). These data indicate that increased vEC proliferation in EAE, rather than sprouting
265 angiogenesis, leads to venous expansion (diameter and coverage). Interestingly, EC proliferation
266 (K67^{+} ECs) was absent in αSMA^{+} CD31^{+} aEC and Mfsd2a^{+} cEC in both control and EAE spinal
267 cords (**Extended Data Figure 4a, b**). Therefore, EC proliferation is restricted to vECs in EAE.
268

269 Endomucin (Emcn) is another integral membrane glycoprotein expressed in cECs and
270 vECs[70] implicated in modulation of VEGF-A-dependent angiogenesis in the retina[71]. Similar to
271 EphB4, Emcn protein was increased in acute EAE spinal cord, relative to control and chronic EAE
272 **(Figure 4g, h)**. These data are consistent with the analysis of differentially expressed genes by
273 scRNAseq showing upregulation in *Emcn* expression in EAE vECs **(Figure 4i)**, but downregulated
274 in diseased cECs. In contrast to ECs, there were no Ki67^{+} pericytes around blood vessels either in
275 control or EAE spinal cords **(Extended Data Figure 4c)**.
276
277 Together, these data support our hypothesis that angiogenesis is unique to vECs in
278 neuroinflammation. The lower vein density observed in chronic compared to acute EAE could be
279 explained, in part, by a sequential specification of a venous (acute) followed by capillary and/or
280 arterial fate (chronic) during disease, similar to postnatal developmental angiogenesis in the brain,
281 or pathological angiogenesis in the retina[72-74].
282
283 Differential gene expression analysis of diseased versus control vECs showed that the top
284 upregulated transcripts in both acute and chronic EAE were angiogenesis and tip cell markers
285 (**Figure 3e**). To validate these scRNA-seq findings *in vivo*, we analyzed expression of four key
286 angiogenic/tip cell markers (*Egfl7*, Mcam, *Ecm1* and *Serpine1*) in spinal cords by fluorescent *in*
287 *situ* hybridization (FISH) and immunofluorescence staining (IF). Epidermal growth factor-like 7
288 (Egfl7) is an ECM-associated protein that promotes angiogenesis in various organs including
289 postnatal brain and retina[75-78]. Differential expression analysis of *Egfl7* expression by scRNA-seq
290 did not show a significant upregulation in diseased relative to control vECs (**Figure 5a**). *Egfl7*
291 mRNA levels were low-to-absent in CFA, but upregulated in inflamed blood vessels near white
292 matter lesions in acute EAE using FISH combined with IF for Caveolin-1 (EC marker; **Figure 5e,**
293 **i**). Melanoma cell adhesion molecule (Mcam), can function as a receptor for Wnt5a, Netrin1,
294 FGF4, VEGF-C, and Wnt1[79], or co-receptor for VEGF-A (together with VEGFR2)[80] to promote
295 angiogenesis. Mcam expression is enriched in proliferating ECs and tip cells of the brain and
296 retina[65]. DE analysis by scRNA-seq showed significant upregulation of *Mcam* mRNA in both
297 acute and chronic EAE vECs (**Figure 5b**). Mcam protein expression was also significantly
298 upregulated in inflamed veins in acute EAE relative to CFA *in vivo* (**Figure 5f-j**). Extracellular
299 matrix protein 1 (Ecm1) is a secreted glycoprotein that exerts its angiogenic function by

300 potentiating epidermal growth factor receptor (EGFR) signaling[81], which regulates synthesis and
301 secretion of other angiogenic factors, including VEGF-A[82]. Differential expression analysis
302 revealed that *Ecm1* mRNA was one of the most significantly upregulated genes in acute, and to a
303 lesser extent, in chronic EAE vECs (**Figure 5c**). Assessment of *Ecm1* mRNA expression in control
304 and EAE spinal cord tissue confirmed significant upregulation in acute EAE veins (**Figure 5g-k**).
305 Finally, the serine protease inhibitor Serpine1 is a specific inhibitor of the plasminogen activation
306 system[83] and plays a crucial role in tumor progression and angiogenesis[84]. Expression of *Serpine1*
307 was also significantly upregulated in acute, and to a lesser extent, chronic EAE vEC (**Figure 5d**).
308 Assessment of *Serpine1* RNA expression *in vivo* revealed a trend toward increased expression in
309 inflamed white matter blood vessels in acute EAE relative to control ($p = 0.1261$; **Figure 5h-l**). In
310 summary, the *in vivo* validation of four angiogenic/tip cell marker expression identified from
311 scRNA-seq confirms that neo-angiogenic genes are highly upregulated in inflamed veins in white
312 matter lesions during peak (acute) EAE, but downregulated in chronic disease.
313
314 **Expression of several angiogenic markers is upregulated in human MS tissue**
315 Previous studies have shown higher vessel density and vessel abnormalities around acute
316 and chronic MS plaques[27,85], with irregular EC morphology[20] and proliferation[21]. However, the
317 molecular mechanisms of neo-angiogenesis in human MS are unknown. We examined expression
318 of several angiogenesis markers, identified from scRNA-seq of Ecs in EAE, in acute or chronic
319 demyelinating plaques within white matter (WM) lesions from16 MS patients, and compared them
320 to either normal appearing white matter (NAMW) within the same tissue, or NAWM from brain
321 samples of 16 non-neurological cases (**Extended Data Table 4**) with immunohistochemistry (12
322 cases per group), or *in situ* hybridization (4 cases per group). The $CD31^+$ vascular coverage (vessel
323 density) was slightly, albeit not significantly, higher inside the WM lesions of MS patients
324 compared to NAWM in non-neurological controls (**Figure 6a-a", d**). However, expression of two
325 angiogenesis markers EGFL7 and MCAM proteins, was increased in blood vessels within WM
326 lesions of MS patients compared to NAWM in non-neurological controls (**Figure 6b-c", e-f**).
327 There was a 4-fold increase in vascular EGFL7 expression and a 2-fold increase in $MCAM^+$
328 vessels in WM lesions from chronic RMMS patients compared to the NAWM of non-neurological
329 controls (**Figure 6e, f**). Expression of mRNAs for *SERPINE1* and *ECM1*, showed a similar pattern
330 to EGFL7 protein (**Extended Data Fig. 5b-c"**). Thus, several molecular markers of pathological

331 angiogenesis, identified from scRNA-seq of Ecs in EAE, are upregulated in demyelinating MS
332 plaques in RRMS cases.
333
334 We asked whether transcriptomic features of pathological neo-angiogenesis are present in
335 SPMS, characterized by progressive neurodegeneration and cumulative disability. We examined
336 expression of neo-angiogenesis markers in SPMS cases using the spatial transcriptomics data from
337 Kaufmann et al., 2022[86]. This study analyzed gene expression within an array of 100-μm diameter
338 spots from MS lesions in SPMS and identified the presence of angiogenesis near MS lesions[86]. We
339 binned all spots by their distance from MS lesion borders in each case, using bins of 0.5 mm width,
340 and calculated the fraction of spots within each bin where neo-angiogenesis genes were detected.
341 White matter (WM) spots near MS lesions showed higher expression for *SERPINE1 and*
342 *MARKSL1* mRNAs, two regulators of angiogenesis[84,87], compared to either gray matter (GM) area
343 near the lesion, or a distant region (sulcus area; **Extended Data Figure 5e, g**). In contrast, *EGFL7*
344 and *ECM1* mRNAs showed higher expression in the GM near the lesion (**Extended Data Figure**
345 **5d, f**). Thus, some molecular markers of pathological neo-angiogenesis are also present in SPMS.
346
347 **Treatment with the anti-VEGF-A monoclonal antibody r84 at the EAE onset downregulates**
348 **transcriptomic features of pathological neo-angiogenesis**
349 Upregulation of VEGF-A and TGF-β signaling in vECs from acute and chronic EAE
350 together with features of neo-angiogenesis (**Figure 3a, c**) implicates their role as potential drivers
351 of neo-angiogenesis in neuroinflammation. In addition to promoting angiogenesis, VEGF-A also
352 induces vascular permeability by triggering the disassembly of adherens and tight junctions in
353 endothelial cells through VEGFR2 phosphorylation and activation[88]. r84 is a fully human anti-
354 VEGF-A monoclonal antibody that binds to both human and mouse VEGF-A and selectively
355 blocks its interactions with VEGFR2 inhibiting tumor angiogenesis[43,44]. To test how effectively
356 r84 inhibits VEGF-A-driven vascular permeability in mouse brain endothelial cells (mBEC), we
357 measured trans-endothelial electrical resistance (TEER) over time (a readout of barrier
358 permeability), in control mBEC and those treated with VEGF-A (100 ng/mL) and a 100-fold molar
359 excess of either r84 or a human IgG isotype control. VEGF-A/IgG treatment induced a significant
360 drop in TEER compared to control (no treatment); this effect was partially rescued by r84 addition
361 (**Extended Data Figure 6a**). Bulk RNA sequencing of control, VEGF-A/IgG, and VEGF-A/r84-

362 treated mBECs revealed significant changes in gene expression and signaling pathway activation
363 as determined by the principal component analysis (PCA), differential expression analysis, and
364 GSEA (**Extended Data Figure 6b; Extended Data Table 2**). VEGF-A increased expression of
365 "pro-angiogenic" and "pro-inflammatory" gene signatures, but decreased expression of "oxidative
366 phosphorylation" signatures; these effects were counteracted by r84 (**Extended Data Figure 6c**).
367 However, r84 treatment did not reduce upregulation of "Wnt/β-catenin signaling" gene signatures
368 driven by VEGF-A treatment in mBECs (**Extended Data Figure 6c**).
369
370 To test whether VEGF-A inhibition reduces transcriptomic features of neo-angiogenesis in
371 EAE and affects clinical outcomes, we administered 5 mg/kg of either r84 or the human IgG1
372 isotype control to EAE mice every 3 days starting at 6 d.p.i. (before disease onset) until tissue
373 collection at chronic stage (28 d.p.i) (**Figure 7a**). r84 treatment lowered the incidence of more
374 severe EAE in mice relative to the IgG (**Figure 7b**), although there was no significant difference
375 in clinical course of EAE, disease onset, peak clinical score and score on the day of collection
376 between two treatments (**Figure 7c-e**). To determine whether r84 treatment suppresses the
377 transcriptomic signatures of neo-angiogenesis in vECs during EAE, we isolated spinal cord ECs
378 from r84- and IgG-treated chronic EAE mice (28 d.p.i.) mice for scRNA-seq analysis [n=3 r84-
379 and 3 IgG-treated chronic EAE samples (6 and 8 mice, respectively)]. All samples were processed
380 in the same batch (**Extended Data Table 1-1**). The clustering of spinal cord ECs isolated from
381 both treatments and visualized with the t-SNE plots (**Figure 7f, g**) reflected the same AV zonation
382 observed without treatment (**Figure 1c-e**) Venous EC (vECs and vnECs), but not aECs or cECs,
383 from the r84-treated EAE mice formed separate clusters from IgG-treated ones (**Figure 7h**). GSEA
384 of differentially expressed genes in r84- versus IgG-treated venous ECs from chronic EAE
385 revealed suppression of gene signatures associated with "angiogenesis", "tip cells", "antigen
386 presentation", and "apoptosis", while upregulation of those related to "BBB" and "canonical Wnt
387 signaling" (**Figure 7i, Extended Data Table 1-10**). BBB genes related to "tight junctions",
388 "transporters", "Wnt/β-catenin signaling", and "transcytosis" were upregulated in vECs, whereas
389 "angiogenic" signatures were downregulated (**Figure 7j, k**). Therefore, r84-treatment suppressed
390 neo-angiogenic transcriptomic signatures in chronic EAE, similar to its effects *in vitro* (**Extended
391 Data Figure 6b)**.
392

393 To understand the effects of r84 treatment on the EAE vascular pathology, we examined
394 whether neo-angiogenesis was reduced in r84-treated spinal cord in chronic EAE. We compared
395 vEC proliferation and venous coverage in chronic EAE spinal cords (28 d.p.i) between r84- and
396 IgG-treated groups. There was a significant reduction in vEC proliferation (Ki67$^+$ Ecs), EphB4$^+$
397 venous coverage and vein diameter in r84- compared to IgG-treated EAE spinal cords (**Figure 8a-**
398 **c, g**). Similarly, the vascular coverage of Endomucin$^+$ vECs was significantly reduced in EAE
399 mice after r84 treatment **(Figure 8d, e)**. Consistent with scRNA-seq results (**Figure 7**), these data
400 demonstrate that neo-angiogenesis (vEC proliferation, increased venous diameter and coverage)
401 observed in EAE was reduced by inhibiting VEGF-A signaling with r84. In contrast, the area of
402 serum IgG and fibrinogen leakage across the BBB in chronic EAE spinal cords were not
403 significantly different between the two groups **(Figure 8d, f; Extended Data Figure 7b, h)**. Thus,
404 although r84 administration reduced neo-angiogenesis in chronic EAE, it did not rescue increased
405 BBB permeability, a critical pathological feature of the vasculature in EAE/MS.
406
407 To understand why r84 treatment did not affect EAE clinical outcome, we examined the
408 number of lesions, extent of demyelination and immune infiltration in r84- and IgG-treated EAE
409 spinal cords. While EC proliferation and venous coverage were downregulated significantly in
410 r84-treated EAE mice (**Figure 8a-c**, **Extended Data Figure 7c**), the number of lesions, the
411 percentage of demyelinated WM area (measured by the absence in fluoromyelin staining), and the
412 number of infiltrating CD4$^+$ T helper cells and the CD68$^+$ infiltrating macrophages, were not
413 significantly different between the two treatment groups (**Extended Data Figure 7a-b, d-g**).
414 Overall, our findings indicate that VEGF-A signaling drives pathological neo-angiogenesis in EAE
415 from vECs. Although its blockade reduces gene signatures and histopathological features of neo-
416 angiogenesis, it is not sufficient to rescue BBB leakage, and consequently immune cell infiltration
417 into the CNS, demyelination and EAE clinical outcomes.
418
419 **DISCUSSION**
420 The presence of neo-angiogenesis and high levels of VEGF-A has been documented in
421 both MS and EAE for several decades[20-23,27,32]. Previous functional studies using monoclonal
422 antibodies (Bevacizumab, B20.4-1-1) to block VEGF-A signaling have concluded that VEGF-A-
423 driven neo-angiogenesis worsens EAE clinical outcomes[26,28]. However, the timing and relation of

424 neo-angiogenesis to EAE/MS progression, its molecular characterization, and the vascular origin
425 and signaling pathways driving neo-angiogenesis in neuroinflammation are poorly understood.
426 Here, we employed scRNA-seq and GSEA, together with fluorescent *in situ* hybridization and
427 immunofluorescence validation to demonstrate that venous ECs, primarily in acute EAE, express
428 transcriptomic signatures of neo-angiogenesis together with activation of pro-angiogenic VEGF-
429 A and TGF-β signaling (**Figure 3**). Thus, venous ECs are the primary EC subtype responsible for
430 pathological angiogenesis in neuroinflammation (**Figure 8h**). Several neo-angiogenesis markers,
431 identified through scRNA-seq in EAE, are also upregulated in human MS lesions from both RRMS
432 and SPMS cases. This upregulation is accompanied by a moderate, albeit not significant, increase
433 in vascular density (**Figure 6; Extended Data Figure 5**). Through functional validation studies,
434 we show that treatment with the VEGF-A blocking antibody r84[43,44] at the disease onset reduces
435 neo-angiogenic transcriptomic signatures and EC proliferation *in vivo*, but does not restore BBB
436 function, or significantly ameliorate EAE pathology. Below, we discuss a putative model for
437 pathological angiogenesis in neuroinflammation and therapeutic implications for MS.
438
439 Prior studies employing bulk or scRNA-seq of the endothelium in EAE have shown that
440 ECs acquire transcriptomic features of inflammation and lose expression of those associated with
441 the BBB[50,51]. Through scRNA-seq and *in vivo* validation, we demonstrate for the first time that
442 transcriptomic signatures and features of angiogenesis arise from vein/venule ECs in
443 neuroinflammation. This was achieved through isolation of sufficient ECs from each vessel
444 subtype from healthy, CFA controls and disease states to identify gene signatures and pathways
445 that were up- and downregulated in neuroinflammation. Since the number of angiogenic ECs
446 arising from vEC/vnECs is small, they were likely missed in previous analyses[50,51]. Nevertheless,
447 the identification of vECs as the source of neuroinflammation-related angiogenesis is somewhat
448 surprising. The classical model suggests that angiogenesis occurs from pre-existing capillaries,
449 whereby cECs respond to a hypoxia-induced VEGF-A gradient and differentiate into migratory
450 tip and proliferating stalk cells that expand the vascular network (reviewed in [89,90]). Recent studies
451 have challenged this dogma. Coelho-Santos *et al*. have shown that CNS angiogenesis in the
452 neonatal mouse brain is initiated from cortical ascending venules[72]. Lee *et al*. have utilized EC
453 vascular subtype-specific inducible reporter mice to fate map ECs in the developing postnatal
454 retinal vasculature, and discovered that ~80% of ECs are of venous origin at both P7 and P25[74].

455 Moreover, neo-angiogenic sprouts arise exclusively from veins in the oxygen-induced retinopathy
456 (OIR) model[74]. Rohlenova *et al.* have employed scRNA-seq and trajectory inference to predict
457 that vECs differentiate into neo-angiogenic tufts during choroidal neovascularization (CNV), a
458 model for wet age-related macular degeneration (AMD)[91]. Their data also suggests that disease-
459 specific EC population, which contains clusters of proliferating and tip ECs, exhibit vein marker
460 expression[91]. Lastly, a recent scRNA-seq study of the lung tumor vasculature has also found that
461 tumors have a higher proportion of vECs, compared to the normal vasculature[63].
462
463 Why are vein/venule, but not arterial/capillary ECs angiogenic in neuroinflammation?
464 Postcapillary venules and veins are the primary sites of immune cell infiltration and BBB damage
465 in MS/EAE[1,2]. Activated T cells that infiltrate into the hypoxic CNS parenchyma secrete VEGF-
466 A[92,93], which can promote angiogenesis locally (**Figure 8h**). Macrophages, which make up a large
467 proportion of cellular infiltrates in MS/EAE also secrete numerous pro-angiogenic factors,
468 including VEGF-A, FGF, PDGF and Angiopoetin-1 and -2[94] (**Figure 8h**). They also produce the
469 matrix metalloproteinases MMP-7 and -9[95], which can digest the ECM surrounding the
470 veins/venules to free ECM-bound VEGF-A, while simultaneously creating a path through the
471 vascular basement membrane for EC migration. Another explanation for the venous origin of neo-
472 angiogenesis in neuroinflammation could be related to differences in shear stress levels present in
473 arteries, capillaries and veins which regulates phosphorylation of VEGFR2, VE-Cadherin, CD31
474 and Erk1/2 (reviewed in[96]). High shear stress in arteries may obstruct EC proliferation and
475 migration, whereas low shear stress in veins may be conducive to neo-angiogenesis.
476
477 Our scRNA-seq analyses of spinal cords ECs from control and EAE mice revealed that
478 gene sets associated with VEGF-A, but not Wnt/β-catenin, signaling and neo-angiogenesis are
479 specifically enriched in vECs in neuroinflammation, implicating VEGF-A as a possible driver of
480 neo-angiogenesis in EAE (**Figure 8h**). Previous studies have shown that administration of VEGF-
481 A inhibitors such as bevacizumab [26], B20-4.1.1[28] or SU5416[24] at the EAE induction improve
482 clinical outcomes in EAE mice. It has been unclear, however, if these VEGF-A inhibitors exert
483 their therapeutic effects directly on CNS angiogenesis in neuroinflammation, or indirectly by
484 dampening the peripheral immune response resulting in less CNS immune infiltration. Treatment
485 with SU5416 (Semaxinib), a potent and selective inhibitor of VEGFR2, reduces immune filtration

486 in the CNS[24]. Similarly, Macmillan *et al.*, have shown that prophylactic administration of
487 bevacizumab (humanized monoclonal antibody) and B20-4.1.1 (monoclonal antibody that binds
488 both human and mouse VEGF-A) prior and throughout EAE onset in mice reduces peripheral T
489 cell responses, decreases $CD4^+$ T cell recruitment into the spinal cord and IL-17A and IFNγ
490 secretion in response to *in vitro* stimulation with MOG_{35-55} [26,28]. However, bevacizumab does not
491 bind murine VEGF-A, and therefore it is puzzling how it improves EAE clinical outcomes[26]. In
492 our study, we used r84, a humanized anti-VEGF-A monoclonal antibody that binds both human
493 and mouse VEGF-A and selectively blocks its interactions with VEGFR2 receptor [43,44] to test the
494 contribution of VEGF-A-mediated neo-angiogenesis in EAE pathology. Our data demonstrate that
495 r84 administration prior to EAE onset reduces transcriptomic signatures and pathological features
496 of neo-angiogenesis including vEC proliferation, increased venous diameter and coverage
497 observed in EAE (**Figure 7**). Although r84 can inhibit acute VEGF-A driven endothelial barrier
498 breakdown *in vitro* **(Extended Data Figure 6a)**, BBB leakage in chronic EAE was not improved
499 by r84 administration **(Figure 8d, f; Extended Data Figure 7b, h)**. This could be due to difference
500 between *in vitro* and *in vivo* inflammatory environments or timing (acute vs chronic). Since
501 increased BBB permeability is a critical pathological feature of EAE that permits immune cell
502 infiltration into the CNS and pathology, there was no significant reduction in T cell or macrophage
503 infiltration, demyelination and EAE clinical outcomes upon r84 administration. Our findings
504 contrast with previously published studies showing that VEGF-A inhibitors such as bevacizumab
505 [26], B20-4.1.1[28] or SU5416[24] can improve clinical outcomes in EAE mice. The B20-4.1.1 treatment
506 regimen in previous studies may have inhibited VEGF-A binding to VEGFR1 and/or soluble
507 VEGFR1 (Flt1/sFlt1), which could affect the amount of VEGF-A available to bind to VEGFR2.
508 This may explain, in part, the difference in clinical outcomes between previous B20-4.1.1 and our
509 r84 treament regimes in EAE. Further in-depth analyses are warranted to identify the key
510 mechanistic differences between these two treatments. Although it is likely that the beneficial
511 effects of bevacizumab in EAE are off-target since it does not bind murine VEGF-A, other VEGF-
512 A inhibitors, such as B20-4.1.1, likely dampen the initial priming of T-cell mediated immunity
513 critical for EAE initiation, since they were administered at the time of EAE induction. Since we
514 have administered r84 at the time of disease onset (day 6), bypassing the initial peripheral immune
515 activation, it is possible that anti-angiogenic therapies in combination with immunomodulatory
516 therapies may benefit MS progression. Further studies are warranted to combine r84 treatment

517 with immunosppressive therapies (that do not affect neo-angiogenesis) to ascertain the effect of
518 this combination therapy in EAE clinical outcome.
519
520 In addition to its role in angiogenesis, VEGF-A is a key regulator of vascular
521 permeability through multiple mechanisms (reviewed in[88]). Activation of VEGF signaling
522 downregulates expression of Claudin-5 and Occludin[97], induces phosphorylation of Occludin and
523 ZO-1[98,99] and disrupts ZO-1 and Occludin organization[100], resulting in TJ disassembly in brain
524 microvascular endothelial cells (BMECs). VEGF-A also promotes VE-cadherin endocytosis and
525 barrier dysfunction[101]. DE analysis revealed that expression of the TJ proteins, Claudin-5,
526 Occludin and ZO-1 (*Tjp1*), were significantly upregulated in vein Ecs after r84 treatment, likely
527 due to inhibition of VEGF-A signaling[102]. Therefore, r84-mediated VEGF-A inhibition in EAE
528 may reduce both vEC neo-angiogenesis and promote restoration of several BBB properties (tight
529 junctions, Wnt/β-catenin signaling, transporters) at the transcriptome level (**Extended Data Fig.
530 5**). However, we show this is not sufficient to restore BBB function, likely due to contribution of
531 other factors (e.g. inflammatory cytokines) in chronic EAE[103].
532
533 In conclusion, our study suggests a model in which VEGF-A derived from either reactive
534 astrocytes[104] or infiltrating immune cells induces neo-angiogenesis from vein ECs in EAE/MS
535 through upregulation of several angiogenic markers such as Egfl7, Emcn, Ecm1, Serpine1 and
536 Mcam which promotes venous EC proliferation, vein diameter expansion and increased vein
537 coverage (**Figure 8h**). Inhibition of VEGF-A signaling with r84 reduces transcriptomic features
538 of neo-angiogenesis (including downregulation of Egfl7, Mcam, Ecm1, Serpine1 and Emcn),
539 without affecting BBB leakage, immune cell activation or their CNS infiltration and EAE clinical
540 outcomes (**Figure 8h**). Several markers of pathogenic angiogenesis identified through our scRNA-
541 seq in EAE are also upregulated in either acute or chronic demyelinating MS plaques in RRMS or
542 in SPMS cases, through *in situ* hybridization analysis and post-hoc spatial transcriptomic analysis
543 of published data[86], respectively. SPMS has no current treatment. Our results advocate for VEGF-
544 A inhibition as a possible therapeutic intervention in the early phases of RRMS to reduce neo-
545 angiogenesis, which may improve long-term neurological deficits in patients as they transition to
546 SPMS.
547

548 **Online Methods**

549

550 **Mice**

551 All experiments were approved by the Institutional Animal Care and Use Committees
552 (IACUC) at Columbia University Irving Medical Center. Animals used for breeding and EAE
553 induction were housed in sex-matched cages of up to five mice in the vivarium with access to food
554 and water *ad libitum*. Wild-type C57BL/6J, obtained from the Jackson Laboratory (Maine), were
555 used for EAE experiments to collect spinal cords from CFA control, acute and chronic EAE for
556 analysis of neo-angiogenesis via immunofluorescence and RNA fluorescent in situ hybridization
557 (FISH). TCF/LEF::H2B::eGFP (Wnt reporter) mice[9,42], purchased from Jackson Laboratory, were
558 used for single-cell RNA sequencing (scRNA-seq) of control and EAE spinal cord endothelial
559 cells (ECs), to track Wnt/β-catenin pathway activation in ECs *post hoc* within the RNA-seq data.
560 The mice were genotyped for GFP with primers [CCCTGAAGTTCATCTGCACCAC (forward);
561 TTCTCGTTGGGGTCTTTGCTC (reverse)] as described[42].

562

563 **Induction of MOG_{35-55} EAE**

564 The induction of MOG_{35-55} EAE in mice has been described[9,42]. Briefly, 10–12-week-old
565 female mice were immunized by subcutaneous injection with 100 μg of myelin oligodendrocyte
566 glycoprotein 35-55 (MEVGWYRSPFSRVVHLYRNGK-COOH) in complete Freund's adjuvant
567 (CFA) containing 200 μg heat killed mycobacterium tuberculosis H37Ra (Difco). 400 ng of
568 *Bordetella pertussis* toxin was administered intravenously at day 0 and day 2. Mice were examined
569 for clinical EAE signs starting at 5 days post immunization (d.p.i) using the scale (0.5-point
570 gradations for intermediate presentation): 0, no signs; 1, flaccid tail; 2, hindlimb paresis; 3,
571 hindlimb paralysis; 4, hindlimb and forelimb paralysis; 5, moribund; 6, death. Control animals
572 immunized with CFA emulsion and pertussis toxin did not exhibit any clinical signs. Spinal cord
573 tissue was collected at the peak acute (16 d.p.i), the beginning of chronic (28 d.p.i), or chronic (40
574 d.p.i) EAE, as well as from healthy and CFA controls, for scRNAseq, immunofluorescence and
575 RNA *in situ* hybridization analyses of angiogenic marker expression.

576

577 **Injection of VEGF-A monoclonal antibodies in EAE**

578 Mice induced with MOG_{35-55} EAE were placed into two groups at 6 d.p.i.: Group 1 (r84-
579 treated) was injected intraperitoneally with 5 mg/kg of the anti-VEGF-A monoclonal antibody,
580 r84[43] every 3 days until tissue collection at 28 d.p.i. Group 2 (IgG-treated) was injected with 5
581 mg/kg of the immunoglobulin G isotype control ([IgG] Biolegend, Cat. # 403502) every 3 days
582 until spinal cord tissue collection at 28 d.p.i. (**Figure 7a**), for analysis of angiogenesis, immune
583 infiltration and leakage, demyelination and scRNA-seq.
584
585 **Isolation of endothelial cells from control and EAE spinal cords**
586 Mice were anesthetized with isoflurane and perfused for 4 minutes with ice-cold sterile
587 PBS. The spinal cord was dissected into Earl's balanced salt solution (EBSS) and dissociated into
588 a single cell suspension using an established protocol[105]. The single cell suspension was
589 resuspended in 200 µl of CD16/CD32 Fc block (BD Biosciences, Cat. # 553141; 1/200 in FACS
590 buffer) and incubated at room temperature for 15 minutes. Samples were washed with 2 ml of
591 FACS buffer, and 100 µl were kept aside for unstained and fluorescence minus one (FMO)
592 controls. The cells were resuspended in 200 µl of anti-CD31-APC (Biolegend, Cat. # 102410;
593 1/200 in FACS buffer) antibody to label endothelial cells (ECs) and incubated on ice in the dark
594 for 30-60 mins. Following antibody labeling, the samples were washed twice with 2 ml of FACS
595 buffer and resuspended in 400 µl of propidium iodide (Thermofisher, Cat. # P1304MP; 1/10,000
596 in FACS buffer). Gates for the surface stain were set using the unstained and FMO controls. The
597 CD31-APC positive ECs were sorted out using the BD FACS Aria Flow Cytometer (Columbia
598 Stem Cell Initiative Flow Cytometry Core) and processed for scRNA-seq.
599
600 **mBEC culture and TEER measurements**
601 Primary mouse brain endothelial cells (mBECs; Cell Biologics C57-6023) were grown to
602 confluency on Poly-D-Lysine (10ug/mL) and Type IV collagen (20ug/mL) coated 96W20idf PET
603 plates (Applied Biophysics), for TEER experiments and 10 cm plates for bulk RNA-seq with
604 complete mouse endothelial cell medium kit (Cell Biologics M1168) and 5% FBS. TEER was
605 measured in real time using an electric cell-substrate impedance sensing (ECIS) instrument
606 (Applied BioPhysics). Once confluency was reached, cells were switched to 1% FBS medium
607 without growth factor supplements. After 24 hours in low serum, cells were treated with control
608 medium, VEGF-A (100ng/mL, Cat #493-MV, Lot #RQ0321011) and Human IgG1 (Bioxcell, Cat

609 #BE0297, Lot #786222A2), or VEGF-A (100ng/mL) and r84 (generated by R. A. Brekken). IgG
610 and r84 were used in 100-fold molar excess as reported[43].
611
612 TEER was measured for 48 hours after treatment (96 hours total). The change in TEER
613 was determined by calculating the average resistance values during a 1-hour period following
614 treatment (acute) and the last 1-hour period of recording (chronic), and then subtracting this value
615 from the average resistance of the well during the 1-hour period prior to treatment. Values were
616 averaged across 8 wells for each condition to generate time course and conditions were compared
617 by unpaired two-tailed Student's t-test. Cells were also collected at 48 hours after treatment and
618 RNA was extracted using Rneasy Mini Kit (QIAGEN) for bulk RNA sequencing.
619
620 **Single-cell RNA sequencing analysis**
621 **Sample Size:** For scRNA-seq, we used two mice per sample to collect sufficient ECs from
622 spinal cords. The sample size was: a) healthy mice: n = 3 samples (n = 6 mice) from which we
623 isolated 4251, 2907, 4531 ECs from each sample; b) CFA disease control: n = 3 samples (n = 6
624 mice) from which we isolated 3377, 4360, 3595 ECs per sample; c) acute EAE: n = 4 samples (n
625 = 8 mice) from which we isolated 2176, 1861, 2002, 1929 ECs per sample; and d) chronic EAE:
626 n = 4 samples (n=8 mice) from which we isolated 3110, 2381, 4603, 4226 ECs per sample. For
627 scRNA-seq of r84- and IgG-treated EAE mice we used 2-4 mice per sample to collect sufficient
628 ECs from spinal cord (IgG: n = 3 samples (8 mice) from which we isolated 2381, 1429 and 2374
629 ECs per sample; r84: n = 3 samples (6 mice) from which we isolated 921, 3456 and 3987 ECs per
630 sample) (**Extended Data Table 1-1**).
631
632 The 10x Genomics Chromium[106,107] platform was used to profile cells (at a median of
633 ~2000 genes/cell), and sequencing data was processed using the Cellranger v3.0 analysis pipeline
634 to align reads and generate feature-barcode matrices. The Seurat R package[45] was used to read the
635 output of the Cell Ranger pipeline and merge data from all the samples (controls and EAE) into a
636 single R object. The standard pre-processing workflow for scRNAseq data was carried out in
637 Seurat, which consisted of the selection and filtration of cells based on quality control metrics
638 (number of unique genes detected in each cell > 200, total number of molecules detected within a
639 cell > 1,000 and < 50,000, percentage of reads within a cell that map to the mitochondrial genome

640 < 20), data normalization and scaling, and the detection of highly variable features. Next, linear
641 dimensionality reduction (PCA) was performed on the scaled data using the previously determined
642 highly variable features (2,000 genes), an alternative heuristic method ('Elbow plot') was
643 implemented to determine the 'dimensionality' of the dataset (resulting in 30 PCs being retained),
644 and cells were clustered by applying the weighted shared nearest-neighbor graph-based clustering
645 method[108] using the first 30 PCs and resolution value 1.5. Lastly, the 30 PCA dimensions were
646 further reduced into two-dimensional space using the non-linear dimensional reduction technique,
647 t-distributed stochastic neighbor embedding (t-SNE), to visualize and explore the scRNA-seq
648 dataset and each of its unique EC clusters. This analysis workflow produced 23 EC clusters. These
649 clusters are not necessarily biologically distinct, as the main purpose of the 'over-clustering' step
650 was to establish clear boundaries between cells belonging to each of the major vessel subtypes
651 (arteries, capillaries, venules, veins) using EC subtype-specific marker gene expression. Cluster-
652 specific expression of these EC subtype-specific genes were then used to assign each of the 23
653 clusters to a major vessel subtype. This approach based on over-clustering and then re-merging
654 based on computational or biological meaning avoids pitfalls arising from incorrect clustering
655 boundaries with lower resolution[47].
656
657 **Differential Gene Expression Analysis**
658 The Seurat "FindMarkers" function with the default Wilcoxon Rank Sum test was
659 implemented to compile the lists of differentially expressed genes, by comparing expression
660 profiles of disease enriched (acute and chronic) EC clusters to control EC clusters, and r84-treated
661 vEC clusters to IgG-treated vEC clusters from chronic EAE.
662
663 **Gene Set Enrichment Analysis (GSEA)**
664 Following DE analysis, a score was calculated for each gene using the formula: Gene score
665 = $-\log_{10}$(pval) x sign ($\log_2$fc). Up- and downregulated genes had a positive and negative score,
666 respectively. The numeric value of the gene score was inversely correlated with the degree of
667 significance, that is, genes that had the highest statistically significant difference in expression and
668 the lowest p-values had the highest score, while non-significant genes with high p-values had a
669 correspondingly low gene score. This score was used to rank each gene in DE gene list (**Extended
670 Data Table 1-3 to 1-10**). New gene sets relevant to pathways, processes and cell types of interest

671 (VEGF-A signaling, canonical Wnt/β-catenin signaling, non-canonical Wnt signaling,
672 chemokine/cytokine signaling, TGF-β signaling, extracellular matrix, cell-cell adhesion,
673 transporters, Notch signaling, angiogenesis, endothelial cell proliferation, endothelial cell
674 migration, apoptosis, antigen processing and presentation, blood-brain barrier, inflammation,
675 endothelial-to-mesenchymal transition, tip cells) were compiled as part of the overall gene set
676 enrichment analysis (**Extended Data Table 1-2)**, using the GO, KEGG, DAVID and GSEA
677 databases as published before[109-111]. The ranked list of DE genes, along with the compiled gene
678 sets, were loaded onto GSEA 4.3.2 software, and run through 'GseaPreranked' with the following
679 settings: Number of permutations = 1,000; Collapse/Remap to gene symbols = No_collapse; Max
680 size: exclude larger sets = 1,500; all other settings were left at 'default'. Gene sets with FDR q-
681 value ≤ 0.10 were deemed significantly enriched (na_pos) or depleted (na_neg) in the cluster of
682 interest (e.g., acute, or chronic EAE EC enriched cluster) relative to its counterpart (e.g., control
683 EC enriched cluster) in the DE analysis, and plotted in the GSEA graphs. Although less rigorous
684 than the standard $p < 0.05$ threshold, the 0.1 threshold is nonetheless the default in GSEA for
685 standard enrichment analyses, so we maintained it here[52].
686
687 **Bulk RNA sequencing**
688 Bulk RNA-seq was performed by JP Sulzberger Columbia Genome Center. mRNA was
689 enriched from total RNA samples using poly-A pull down and cDNA libraries were prepared using
690 Illumina Truseq chemistry, followed by sequencing using Illumina NovaSeq 6000.
691 Pseudoalignment of RNAseq reads was performed to a kallisto index created from transcriptome
692 Ensembl v96, Mouse:GRCm38.p6 using kallisto (0.44.0). Differential gene expression analysis
693 between control, VEGF-A/IgG, and VEGF-A/r84-treated samples was performed using DESeq2.
694 Gene set enrichment analysis was performed using endothelial cell curated and hallmark gene sets.
695 For heat map visualization, size factors were calculated using a median ratio method to normalize
696 raw gene counts across samples (to adjust for differences in sequencing depth and library size) and
697 z-scores were calculated for each gene's normalized counts. To further assess overall similarity
698 between samples, regularized logarithm transformation was performed on differentially expressed
699 genes and principal component analysis was performed on transformed expression data.
700
701 **Immunofluorescence analysis**

702 Mice used for immunofluorescence staining were anesthetized with isoflurane and
703 perfused with PBS for 4 minutes followed by 4% PFA for 6 minutes. Spinal cords were extracted
704 and post-fixed for 2 hours, washed three times in PBS for 30 minutes, then cryoprotected in 30%
705 sucrose overnight and embedded in Tissue Plus O.C.T. Compound (Fisher Scientific, Cat # 4585).
706 The tissue blocks were stored at -80 °C until use. Tissues were then sectioned at 12 µm on a Leica
707 cryostat and stored at -80 °C until use. For staining, slides were air-dried for 20 minutes then placed
708 horizontally in a humidified chamber. Slides were washed once in PBS for 10 minutes to remove
709 excess OCT, then blocked for 1 hour in blocking buffer (10% BSA, 0.1% Triton-X-100 in 1x
710 PBS). Primary antibodies (**Extended Data Table 3**) were diluted in 0.1% Triton-X-100 in PBS
711 with 1% BSA. Primary antibody solutions were incubated overnight at 4 °C. Slides were washed
712 three times for ten minutes with PBST (0.1% Triton-X-100 in PBS), then primary antibodies were
713 targeted using associated fluorescently tagged secondary antibodies (1:1000 for Alexa488 and
714 Alexa594, 1:500 for Alexa647). Secondary antibodies were diluted in PBST and incubated for two
715 hours at room temperature. Nuclei were then labeled with DAPI (4′,6-diamidino-2-phenylindole,
716 1:20,000 in PBST) for 10 minutes, then slides were washed twice with PBST and twice with PBS.
717 Slides were mounted with Vectashield (Vector Labs, Cat # H-1000), coverslipped and sealed with
718 clear nail polish, and stored at -20 °C. Imaging of brain sections were performed with either a Zeiss
719 LSM700 confocal microscope or a Zeiss AxioImager.
720
721 **Chromogenic immunohistochemistry of human tissue**
722 Formalin-fixed human brain samples were obtained from the NIH Brain & Tissue
723 Repository-California, Human Brain & Spinal Fluid Resource Center at the Veterans Affairs
724 Hospital West Los Angeles Healthcare Center, Los Angeles, California, which is supported in part
725 by National Institutes of Health and the US Department of Veterans Affairs under the CUIMC
726 IRB protocol # AAAQ7343. Brain tissues from 16 MS and 16 non-neurological control patients
727 were used in this study (**Extended Data Table 4**). Upon receipt, the fixed samples were washed
728 with cold PBS then dehydrated in 30% sucrose before embedding in Tissue-Tek O.C.T. Compound
729 (Sakura; Torrance, CA) and cryosectioned 12 µm thick. Single target immune-peroxidase staining
730 was performed as described[42]. Hematoxylin counterstain was used for all stains except for CD31.
731 For 2-target immune-peroxidase staining, targeting both CD31 and Ki67, the ImmPRESS Duet
732 Double Staining Polymer kit (Vector Labs, Cat. # MP-7724, Burlingame, CA) was used, according

733 to manufacturer's recommendations. No nuclear counterstain was used in these experiments. All
734 primary antibodies were diluted in 1% bovine serum albumin, 0.1% Triton-X, in PBS. Images
735 were acquired with a Zeiss Axioimager using a color camera and 10X objective.
736
737 ***In situ* hybridization**
738 Digoxigenin-labeled probes were synthesized from plasmids obtained from TransOMIC
739 using the Roche Applied Science *in vitro* transcription kit (Sigma, 11175025910). The probes used
740 for these experiments are listed in **Extended Data Table 5**. Mice used for *in situ* hybridization
741 experiments were perfused with PBS only, brains and spinal cords were dissected out, embedded
742 in OCT and frozen on dry ice, then stored at -80 °C. Sections were cut onto glass slides using a
743 cryostat. Alkaline Phosphatase *in situ* hybridizations and fluorescent *in situ* hybridization (FISH)
744 combined with immunofluorescence for vascular markers were performed as previously
745 described[42,112]. Slides were imaged either on a Zeiss AxioImager, or an Zeiss LSM700 confocal
746 microscope.
747
748 **Image analysis**
749 Images were prepared and analyzed using ImageJ/FIJI software. For fluorescence
750 measurements, at least three sections were imaged per sample, and in each case, multiple (8-12)
751 representative regions of interest (ROIs) were acquired using the confocal microscope (20x
752 objective). For each ROI, multiple Z-stacks were acquired, and maximal projection was performed
753 in ImageJ to properly capture the full depth of the CNS blood vessels. Background correction was
754 performed in ImageJ when required. For statistical analysis, the mean value for each animal was
755 calculated as the mean signal from all acquired ROIs.
756
757 <u>*Analysis of vein EC proliferation and vein density*</u>: Spinal cord tissue sections were stained
758 with the Ki67 (proliferation marker), EphB4 (vein and venule marker), along with a vascular
759 marker (Caveolin-1/Lectin) and DAPI (**Extended Data Table 4**). $Ki67^{+}$ venous nuclei were
760 counted and normalized to the total venous area to get a readout of EC proliferation rate. The
761 percentage area coverage (readout of vein density) by EphB4+ or Endomucin+ veins and venules
762 over a vascular marker (Caveolin-1/Lectin) was quantified using ImageJ/FIJI.
763

764 *Analysis of angiogenic marker expression*: Spinal cord tissue sections were analyzed for
765 the expression of angiogenic markers (Egfl7, Mcam, Ecm1 and Serpine1) and vessel/vein marker
766 (Caveolin-1/Vcam1) with either FISH combined with immunofluorescence or
767 immunofluorescence staining. The vessel area was outlined by signal thresholding using the
768 ImageJ/FIJI software, and the mean fluorescence intensity (M.F.I.) of angiogenic marker
769 expression within the vasculature was measured using the histogram analysis feature.
770

771 **Statistical analyses**

772 Statistical analyses of EAE disease course and parameters (day of disease onset, peak
773 disease score and score on the day of collection), vascular subtype cell proportions within the
774 scRNAseq data, vein EC proliferation and vein density, angiogenic marker expression and flow
775 cytometry data were performed using GraphPad Prism. Gene set enrichment analysis was
776 performed using the GSEA v4.3.2 Mac App. Data were analyzed by Student's t-test, one-way,
777 two-way, or repeated measures (RM) ANOVA followed by Sidak's, Tukey's, or Bonferroni's
778 post-hoc corrections. Significance (α) was set at 0.05. Data in the dotted bar graphs are represented
779 as mean ± SEM, where each dot is the mean value from each animal.
780

781 **Data availability**

782 The raw and analyzed mouse endothelial scRNA-seq and bulk RNA-seq datasets
783 supporting this manuscript are archived at the NIH GEO repository under accession number
784 GSE210776.
785

786 **Acknowledgements**

787 We thank Jeroen Bastiaans and Heidi Stuhlmann at Weill Cornell Medical College, New
788 York for providing the mouse Egfl7 mRNA probe, and help optimizing the staining of the human
789 tissue with the EGFL7 protein, Tyler Cutforth for advice with the preparation of mRNA probes
790 and FISH experiments, Michael Kissner at the Columbia Stem Cell Initiative Flow Cytometry
791 Core and Erin Bush at the Columbia Single-Cell RNA-sequencing facility for their advice and help
792 with FACS isolation and single-cell RNA-sequencing experiments, respectively.
793

794 **Author Contributions**

Conceptualization: S.S., V.M., D.A.; Methodology: S.S., S.B., V.M., D.A.; Software: S.S., M.C.T., V.M.; Validation: S.S., S.B.; Formal analysis: S.S., S.B., U.A, M.C.T., M.D.G., A.K., C.R.W., G.P., M.Z.P.; Investigation: S.S., S.B., U.A, M.C.T., M.D.G., A.K., C.R.W., G.P., M.Z.P.; Resources: V.M., R.A.B. D.A.; Data curation: S.S., S.B., V.M., D.A.; Writing - revised draft: S.S., S.B., V.M., D.A.; Writing & editing: S.S., S.B., M.C.T., V.M., D.A.; Visualization: S.S., S.B., C.W.; Supervision: V.M., D.A.; Project administration: D.A.; Funding acquisition: V.M., D.A.

COMPETING INTERESTS

The authors declare that the research was conducted without any commercial or financial relationships that can be construed as potential conflicts of interest.

FUNDING

The work was supported mainly by a grant from the National Multiple Sclerosis Society (RG-1901-33218) and in part by several NIH grants [NIMH (R01 MH112849), NEI (R01 EY033994), NHLBI (R61HL159949), NINDS (R21 NS118891; R21NS130265). This research made use of the Genomics and High Throughput Screening Shared Resource, and was funded in part through the NIH/NCI Cancer Center Support Grant P30CA013696.

MATERIALS AND CORRESPONDENCE

The materials are available upon request to Dritan Agalliu.

816 **REFERENCES**

817 1 Daneman, R. & Engelhardt, B. Brain barriers in health and disease. *Neurobiology of*
818 *disease* **107**, 1-3 (2017).
819 2 Liebner, S. *et al.* Functional morphology of the blood-brain barrier in health and disease.
820 *Acta Neuropathol* **135**, 311-336, doi:10.1007/s00401-018-1815-1 (2018).
821 3 Kirk, J., Plumb, J., Mirakhur, M. & McQuaid, S. Tight junctional abnormality in multiple
822 sclerosis white matter affects all calibres of vessel and is associated with blood-brain
823 barrier leakage and active demyelination. *The Journal of pathology* **201**, 319-327 (2003).
824 4 Pan, W., Banks, W. A., Kennedy, M. K., Gutierrez, E. G. & Kastin, A. J. Differential
825 permeability of the BBB in acute EAE: enhanced transport of TNT-alpha. *The American*
826 *journal of physiology* **271**, E636-642 (1996).
827 5 Brown, A., McFarlin, D. E. & Raine, C. S. Chronologic neuropathology of relapsing
828 experimental allergic encephalomyelitis in the mouse. *Laboratory investigation; a journal*
829 *of technical methods and pathology* **46**, 171-185 (1982).
830 6 Alvarez, J. I. *et al.* Focal disturbances in the blood-brain barrier are associated with
831 formation of neuroinflammatory lesions. *Neurobiol Dis* **74**, 14-24,
832 doi:10.1016/j.nbd.2014.09.016 (2015).
833 7 Lossinsky, A. S., Badmajew, V., Robson, J. A., Moretz, R. C. & Wisniewski, H. M. Sites
834 of egress of inflammatory cells and horseradish peroxidase transport across the blood-brain
835 barrier in a murine model of chronic relapsing experimental allergic encephalomyelitis.
836 *Acta Neuropathol* **78**, 359-371 (1989).
837 8 Maggi, P. *et al.* The formation of inflammatory demyelinated lesions in cerebral white
838 matter. *Ann Neurol* **76**, 594-608, doi:10.1002/ana.24242 (2014).
839 9 Lutz, S. E. *et al.* Caveolin1 is required for Th1 cell infiltration, but not tight junction
840 remodeling, at the blood-brain barrier in autoimmune neuroinflammation. *Cell reports* **21**,
841 2104-2117 (2017).
842 10 Plumb, J., McQuaid, S., Mirakhur, M. & Kirk, J. Abnormal endothelial tight junctions in
843 active lesions and normal-appearing white matter in multiple sclerosis. *Brain pathology*
844 *(Zurich, Switzerland)* **12**, 154-169 (2002).
845 11 Kermode, A. G. *et al.* Breakdown of the blood-brain barrier precedes symptoms and other
846 MRI signs of new lesions in multiple sclerosis. Pathogenetic and clinical implications.
847 *Brain : a journal of neurology* **113 (Pt 5)**, 1477-1489 (1990).
848 12 Reijerkerk, A. *et al.* Tissue-type plasminogen activator is a regulator of monocyte
849 diapedesis through the brain endothelial barrier. *Journal of immunology (Baltimore, Md. :*
850 *1950)* **181**, 3567-3574 (2008).
851 13 Winger, R. C., Koblinski, J. E., Kanda, T., Ransohoff, R. M. & Muller, W. A. Rapid
852 remodeling of tight junctions during paracellular diapedesis in a human model of the blood-
853 brain barrier. *Journal of immunology (Baltimore, Md. : 1950)* **193**, 2427-2437,
854 doi:10.4049/jimmunol.1400700 (2014).
855 14 Aube, B. *et al.* Neutrophils mediate blood-spinal cord barrier disruption in demyelinating
856 neuroinflammatory diseases. *Journal of immunology (Baltimore, Md. : 1950)* **193**, 2438-
857 2454, doi:10.4049/jimmunol.1400401 (2014).
858 15 Abadier, M. *et al.* Cell surface levels of endothelial ICAM-1 influence the transcellular or
859 paracellular T-cell diapedesis across the blood-brain barrier. *European journal of*
860 *immunology* **45**, 1043-1058, doi:10.1002/eji.201445125 (2015).

16 Lake, B. B. *et al.* Integrative single-cell analysis of transcriptional and epigenetic states in the human adult brain. *Nature Biotechnology* **36**, 70-80, doi:10.1038/nbt.4038 (2018).
17 Biswas, S., Cottarelli, A. & Agalliu, D. Neuronal and glial regulation of CNS angiogenesis and barriergenesis. *Development* **147**, dev182279 (2020).
18 Girolamo, F., Coppola, C., Ribatti, D. & Trojano, M. Angiogenesis in multiple sclerosis and experimental autoimmune encephalomyelitis. *Acta neuropathologica communications* **2**, 1-17 (2014).
19 Lengfeld, J., Cutforth, T. & Agalliu, D. The role of angiogenesis in the pathology of multiple sclerosis. *Vascular cell* **6**, 1-6 (2014).
20 Proescholdt, M. A., Jacobson, S., Tresser, N., Oldfield, E. H. & Merrill, M. J. Vascular endothelial growth factor is expressed in multiple sclerosis plaques and can induce inflammatory lesions in experimental allergic encephalomyelitis rats. *Journal of neuropathology and experimental neurology* **61**, 914-925 (2002).
21 Holley, J. E., Newcombe, J., Whatmore, J. L. & Gutowski, N. J. Increased blood vessel density and endothelial cell proliferation in multiple sclerosis cerebral white matter. *Neurosci Lett* **470**, 65-70, doi:10.1016/j.neulet.2009.12.059 (2010).
22 Seabrook, T. J. *et al.* Angiogenesis is present in experimental autoimmune encephalomyelitis and pro-angiogenic factors are increased in multiple sclerosis lesions. *J Neuroinflammation* **7**, 95, doi:10.1186/1742-2094-7-95 (2010).
23 Kirk, S. L. & Karlik, S. J. VEGF and vascular changes in chronic neuroinflammation. *J Autoimmun* **21**, 353-363 (2003).
24 Roscoe, W. A., Welsh, M. E., Carter, D. E. & Karlik, S. J. VEGF and angiogenesis in acute and chronic MOG((35-55)) peptide induced EAE. *J Neuroimmunol* **209**, 6-15, doi:10.1016/j.jneuroim.2009.01.009 (2009).
25 Boroujerdi, A., Welser-Alves, J. V. & Milner, R. Extensive vascular remodeling in the spinal cord of pre-symptomatic experimental autoimmune encephalomyelitis mice; increased vessel expression of fibronectin and the alpha5beta1 integrin. *Exp Neurol* **250**, 43-51, doi:10.1016/j.expneurol.2013.09.009 (2013).
26 MacMillan, C. J. *et al.* Bevacizumab diminishes experimental autoimmune encephalomyelitis by inhibiting spinal cord angiogenesis and reducing peripheral T-cell responses. *J Neuropathol Exp Neurol* **71**, 983-999, doi:10.1097/NEN.0b013e3182724831 (2012).
27 Buch, S. *et al.* Revealing vascular abnormalities and measuring small vessel density in multiple sclerosis lesions using USPIO. *Neuroimage Clin* **29**, 102525, doi:10.1016/j.nicl.2020.102525 (2021).
28 MacMillan, C. J. *et al.* Murine experimental autoimmune encephalomyelitis is diminished by treatment with the angiogenesis inhibitors B20-4.1. 1 and angiostatin (K1-3). *PLoS One* **9**, e89770 (2014).
29 Matsumoto, K. & Ema, M. Roles of VEGF-A signalling in development, regeneration, and tumours. *The Journal of Biochemistry* **156**, 1-10 (2014).
30 Carmeliet, P. VEGF as a key mediator of angiogenesis in cancer. *Oncology* **69**, 4-10 (2005).
31 Campochiaro, P. A. Molecular pathogenesis of retinal and choroidal vascular diseases. *Progress in retinal and eye research* **49**, 67-81 (2015).
32 Su, J. J. *et al.* Upregulation of vascular growth factors in multiple sclerosis: correlation with MRI findings. *Journal of the neurological sciences* **243**, 21-30 (2006).

907 33 Presta, L. G. *et al.* Humanization of an anti-vascular endothelial growth factor monoclonal
908 antibody for the therapy of solid tumors and other disorders. *Cancer research* **57**, 4593-
909 4599 (1997).
910 34 Ferrara, N., Hillan, K. J., Gerber, H.-P. & Novotny, W. Discovery and development of
911 bevacizumab, an anti-VEGF antibody for treating cancer. *Nature reviews Drug discovery*
912 **3**, 391-400 (2004).
913 35 Ferrara, N., Hillan, K. J. & Novotny, W. Bevacizumab (Avastin), a humanized anti-VEGF
914 monoclonal antibody for cancer therapy. *Biochemical and biophysical research*
915 *communications* **333**, 328-335 (2005).
916 36 Li, Y.-L., Zhao, H. & Ren, X.-B. Relationship of VEGF/VEGFR with immune and cancer
917 cells: staggering or forward? *Cancer biology & medicine* **13**, 206 (2016).
918 37 Daneman, R. *et al.* Wnt/β-catenin signaling is required for CNS, but not non-CNS,
919 angiogenesis. *Proceedings of the National Academy of Sciences* **106**, 641-646 (2009).
920 38 Stenman, J. M. *et al.* Canonical Wnt signaling regulates organ-specific assembly and
921 differentiation of CNS vasculature. *Science* **322**, 1247-1250 (2008).
922 39 Liebner, S. *et al.* Wnt/β-catenin signaling controls development of the blood–brain barrier.
923 *Journal of Cell Biology* **183**, 409-417 (2008).
924 40 Zhou, Y. *et al.* Canonical WNT signaling components in vascular development and barrier
925 formation. *The Journal of clinical investigation* **124**, 3825-3846 (2014).
926 41 Tran, K. A. *et al.* Endothelial β-catenin signaling is required for maintaining adult blood–
927 brain barrier integrity and central nervous system homeostasis. *Circulation* **133**, 177-186
928 (2016).
929 42 Lengfeld, J. E. *et al.* Endothelial Wnt/beta-catenin signaling reduces immune cell
930 infiltration in multiple sclerosis. *Proceedings of the National Academy of Sciences of the*
931 *United States of America*, doi:10.1073/pnas.1609905114 (2017).
932 43 Sullivan, L. A. *et al.* r84, a novel therapeutic antibody against mouse and human VEGF
933 with potent anti-tumor activity and limited toxicity induction. *PloS one* **5**, e12031 (2010).
934 44 Roland, C. L. *et al.* Inhibition of vascular endothelial growth factor reduces angiogenesis
935 and modulates immune cell infiltration of orthotopic breast cancer xenografts. *Mol Cancer*
936 *Ther* **8**, 1761-1771, doi:10.1158/1535-7163.MCT-09-0280 (2009).
937 45 Hao, Y. *et al.* Integrated analysis of multimodal single-cell data. *Cell* (2021).
938 46 Vanlandewijck, M. *et al.* A molecular atlas of cell types and zonation in the brain
939 vasculature. *Nature* **554**, 475-480 (2018).
940 47 Miao, Z. *et al.* Putative cell type discovery from single-cell gene expression data. *Nature*
941 *methods* **17**, 621-628, doi:10.1038/s41592-020-0825-9 (2020).
942 48 Halpern, K. B. *et al.* Single-cell spatial reconstruction reveals global division of labour in
943 the mammalian liver. *Nature* **542**, 352-356 (2017).
944 49 Korsunsky, I. *et al.* Fast, sensitive and accurate integration of single-cell data with
945 Harmony. *Nature methods* **16**, 1289-1296, doi:10.1038/s41592-019-0619-0 (2019).
946 50 Munji, R. N. *et al.* Profiling the mouse brain endothelial transcriptome in health and disease
947 models reveals a core blood-brain barrier dysfunction module. *Nat Neurosci* **22**, 1892-
948 1902, doi:10.1038/s41593-019-0497-x (2019).
949 51 Jeong, H.-W. *et al.* Single-cell transcriptomics reveals functionally specialized vascular
950 endothelium in brain. *eLife* **11**, e57520, doi:10.7554/eLife.57520 (2022).

951 52 Subramanian, A. *et al.* Gene set enrichment analysis: a knowledge-based approach for
952 interpreting genome-wide expression profiles. *Proceedings of the National Academy of*
953 *Sciences* **102**, 15545-15550 (2005).
954 53 Zarkada, G. *et al.* Specialized endothelial tip cells guide neuroretina vascularization and
955 blood-retina-barrier formation. *Developmental Cell* **56**, 2237-2251. e2236 (2021).
956 54 Zhao, Q. *et al.* Single-cell transcriptome analyses reveal endothelial cell heterogeneity in
957 tumors and changes following antiangiogenic treatment. *Cancer research* **78**, 2370-2382
958 (2018).
959 55 Conway, E. M., Collen, D. & Carmeliet, P. Molecular mechanisms of blood vessel growth.
960 *Cardiovascular research* **49**, 507-521 (2001).
961 56 Potenta, S., Zeisberg, E. & Kalluri, R. The role of endothelial-to-mesenchymal transition
962 in cancer progression. *British journal of cancer* **99**, 1375-1379 (2008).
963 57 Platel, V., Faure, S., Corre, I. & Clere, N. Endothelial-to-mesenchymal transition
964 (EndoMT): roles in tumorigenesis, metastatic extravasation and therapy resistance. *Journal*
965 *of oncology* **2019** (2019).
966 58 Neve, A., Cantatore, F. P., Maruotti, N., Corrado, A. & Ribatti, D. Extracellular matrix
967 modulates angiogenesis in physiological and pathological conditions. *BioMed research*
968 *international* **2014** (2014).
969 59 Clere, N., Renault, S. & Corre, I. Endothelial-to-mesenchymal transition in cancer.
970 *Frontiers in Cell and Developmental Biology* **8** (2020).
971 60 Hogan, K. A., Ambler, C. A., Chapman, D. L. & Bautch, V. L. The neural tube patterns
972 vessels developmentally using the VEGF signaling pathway. (2004).
973 61 James, J. M., Gewolb, C. & Bautch, V. L. Neurovascular development uses VEGF-A
974 signaling to regulate blood vessel ingression into the neural tube. (2009).
975 62 Nguyen, H.-L. *et al.* TGF-β signaling in endothelial cells, but not neuroepithelial cells, is
976 essential for cerebral vascular development. *Laboratory investigation* **91**, 1554-1563
977 (2011).
978 63 Goveia, J. *et al.* An integrated gene expression landscape profiling approach to identify
979 lung tumor endothelial cell heterogeneity and angiogenic candidates. *Cancer cell* **37**, 21-
980 36. e13 (2020).
981 64 Hupe, M. *et al.* Gene expression profiles of brain endothelial cells during embryonic
982 development at bulk and single-cell levels. *Science Signaling* **10** (2017).
983 65 Sabbagh, M. F. *et al.* Transcriptional and epigenomic landscapes of CNS and non-CNS
984 vascular endothelial cells. *elife* **7**, e36187 (2018).
985 66 del Toro, R. *et al.* Identification and functional analysis of endothelial tip cell–enriched
986 genes. *Blood, The Journal of the American Society of Hematology* **116**, 4025-4033 (2010).
987 67 Wang, H. U., Chen, Z.-F. & Anderson, D. J. Molecular distinction and angiogenic
988 interaction between embryonic arteries and veins revealed by ephrin-B2 and its receptor
989 Eph-B4. *Cell* **93**, 741-753 (1998).
990 68 Davies, M. H., Stempel, A. J., Hubert, K. E. & Powers, M. R. Altered vascular expression
991 of EphrinB2 and EphB4 in a model of oxygen-induced retinopathy. *Developmental*
992 *Dynamics* **239**, 1695-1707 (2010).
993 69 Crist, A. M., Young, C. & Meadows, S. M. Characterization of arteriovenous identity in
994 the developing neonate mouse retina. *Gene Expression Patterns* **23**, 22-31 (2017).
995 70 Zhang, G., Yang, X. & Gao, R. Research progress on the structure and function of
996 endomucin. *Animal Models and Experimental Medicine* **3**, 325-329 (2020).

997 71 Park-Windhol, C. *et al.* Endomucin inhibits VEGF-induced endothelial cell migration,
998 growth, and morphogenesis by modulating VEGFR2 signaling. *Scientific reports* **7**, 1-13
999 (2017).
1000 72 Coelho-Santos, V., Berthiaume, A.-A., Ornelas, S., Stuhlmann, H. & Shih, A. Y. Imaging
1001 the construction of capillary networks in the neonatal mouse brain. *Proceedings of the*
1002 *National Academy of Sciences* **118** (2021).
1003 73 Uemura, A., Kusuhara, S., Katsuta, H. & Nishikawa, S.-I. Angiogenesis in the mouse
1004 retina: a model system for experimental manipulation. *Experimental cell research* **312**,
1005 676-683 (2006).
1006 74 Lee, H.-W. *et al.* The Role of Venous Endothelial Cells in Developmental and Pathologic
1007 Angiogenesis. *Circulation* (2021).
1008 75 Schmidt, M. *et al.* EGFL7 regulates the collective migration of endothelial cells by
1009 restricting their spatial distribution. (2007).
1010 76 Parker, L. H. *et al.* The endothelial-cell-derived secreted factor Egfl7 regulates vascular
1011 tube formation. *Nature* **428**, 754-758 (2004).
1012 77 Nichol, D. *et al.* Impaired angiogenesis and altered Notch signaling in mice overexpressing
1013 endothelial Egfl7. *Blood, The Journal of the American Society of Hematology* **116**, 6133-
1014 6143 (2010).
1015 78 Poissonnier, L., Villain, G., Soncin, F. & Mattot, V. Egfl7 is differentially expressed in
1016 arteries and veins during retinal vascular development. *PloS one* **9**, e90455 (2014).
1017 79 Joshkon, A. *et al.* Role of CD146 (MCAM) in Physiological and Pathological
1018 Angiogenesis—Contribution of New Antibodies for Therapy. *Biomedicines* **8**, 633 (2020).
1019 80 Jiang, T. *et al.* CD146 is a coreceptor for VEGFR-2 in tumor angiogenesis. *Blood, The*
1020 *Journal of the American Society of Hematology* **120**, 2330-2339 (2012).
1021 81 Lee, K.-m. *et al.* Extracellular matrix protein 1 regulates cell proliferation and trastuzumab
1022 resistance through activation of epidermal growth factor signaling. *Breast Cancer*
1023 *Research* **16**, 1-17 (2014).
1024 82 De Luca, A. *et al.* The role of the EGFR signaling in tumor microenvironment. *Journal of*
1025 *cellular physiology* **214**, 559-567 (2008).
1026 83 Stoppelli, M. P. in *Madame Curie Bioscience Database [Internet]* (Landes Bioscience,
1027 2013).
1028 84 Takayama, Y. *et al.* Inhibition of PAI-1 limits tumor angiogenesis regardless of angiogenic
1029 stimuli in malignant pleural mesothelioma. *Cancer research* **76**, 3285-3294 (2016).
1030 85 Girolamo, F., Coppola, C., Ribatti, D. & Trojano, M. Angiogenesis in multiple sclerosis
1031 and experimental autoimmune encephalomyelitis. *Acta Neuropathol Commun* **2**, 84,
1032 doi:10.1186/s40478-014-0084-z (2014).
1033 86 Kaufmann, M. *et al.* Identification of early neurodegenerative pathways in progressive
1034 multiple sclerosis. *Nat Neurosci* **25**, 944-955, doi:10.1038/s41593-022-01097-3 (2022).
1035 87 Kim, B. R. *et al.* MARCKSL1 exhibits anti-angiogenic effects through suppression of
1036 VEGFR-2-dependent Akt/PDK-1/mTOR phosphorylation. *Oncol Rep* **35**, 1041-1048,
1037 doi:10.3892/or.2015.4408 (2016).
1038 88 Venkatraman, L. & Claesson-Welsh, L. in *Tumor Angiogenesis: A Key Target for Cancer*
1039 *Therapy* (ed Dieter Marmé) 33-50 (Springer International Publishing, 2019).
1040 89 Potente, M., Gerhardt, H. & Carmeliet, P. Basic and therapeutic aspects of angiogenesis.
1041 *Cell* **146**, 873-887, doi:10.1016/j.cell.2011.08.039 (2011).

1042 90 Potente, M. & Carmeliet, P. The Link Between Angiogenesis and Endothelial Metabolism.
1043 *Annu Rev Physiol* **79**, 43-66, doi:10.1146/annurev-physiol-021115-105134 (2017).
1044 91 Rohlenova, K. *et al.* Single-Cell RNA Sequencing Maps Endothelial Metabolic Plasticity
1045 in Pathological Angiogenesis. *Cell Metab* **31**, 862-877 e814,
1046 doi:10.1016/j.cmet.2020.03.009 (2020).
1047 92 Gavalas, N. G. *et al.* VEGF directly suppresses activation of T cells from ascites secondary
1048 to ovarian cancer via VEGF receptor type 2. *British Journal of Cancer* **107**, 1869-1875,
1049 doi:10.1038/bjc.2012.468 (2012).
1050 93 Bourhis, M., Palle, J., Galy-Fauroux, I. & Terme, M. Direct and Indirect Modulation of T
1051 Cells by VEGF-A Counteracted by Anti-Angiogenic Treatment. *Front Immunol* **12**,
1052 616837, doi:10.3389/fimmu.2021.616837 (2021).
1053 94 Jetten, N. *et al.* Anti-inflammatory M2, but not pro-inflammatory M1 macrophages
1054 promote angiogenesis in vivo. *Angiogenesis* **17**, 109-118 (2014).
1055 95 Quiding-Järbrink, M., Smith, D. A. & Bancroft, G. J. Production of matrix
1056 metalloproteinases in response to mycobacterial infection. *Infection and immunity* **69**,
1057 5661-5670, doi:10.1128/iai.69.9.5661-5670.2001 (2001).
1058 96 Conway, D. E. & Schwartz, M. A. Mechanotransduction of shear stress occurs through
1059 changes in VE-cadherin and PECAM-1 tension: implications for cell migration. *Cell Adh*
1060 *Migr* **9**, 335-339, doi:10.4161/19336918.2014.968498 (2015).
1061 97 Argaw, A. T., Gurfein, B. T., Zhang, Y., Zameer, A. & John, G. R. VEGF-mediated
1062 disruption of endothelial CLN-5 promotes blood-brain barrier breakdown. *Proceedings of*
1063 *the National Academy of Sciences* **106**, 1977-1982 (2009).
1064 98 Antonetti, D. A., Barber, A. J., Hollinger, L. A., Wolpert, E. B. & Gardner, T. W. Vascular
1065 endothelial growth factor induces rapid phosphorylation of tight junction proteins occludin
1066 and zonula occluden 1: a potential mechanism for vascular permeability in diabetic
1067 retinopathy and tumors. *Journal of Biological Chemistry* **274**, 23463-23467 (1999).
1068 99 Murakami, T., Felinski, E. A. & Antonetti, D. A. Occludin phosphorylation and
1069 ubiquitination regulate tight junction trafficking and vascular endothelial growth factor-
1070 induced permeability. *Journal of Biological Chemistry* **284**, 21036-21046 (2009).
1071 100 Wang, W., Dentler, W. L. & Borchardt, R. T. VEGF increases BMEC monolayer
1072 permeability by affecting occludin expression and tight junction assembly. *American*
1073 *Journal of Physiology-Heart and Circulatory Physiology* **280**, H434-H440 (2001).
1074 101 Gavard, J. & Gutkind, J. S. VEGF controls endothelial-cell permeability by promoting the
1075 β-arrestin-dependent endocytosis of VE-cadherin. *Nature cell biology* **8**, 1223-1234
1076 (2006).
1077 102 Senger, D. R. *et al.* Tumor cells secrete a vascular permeability factor that promotes
1078 accumulation of ascites fluid. *Science* **219**, 983-985 (1983).
1079 103 Lopes Pinheiro, M. A. *et al.* Immune cell trafficking across the barriers of the central
1080 nervous system in multiple sclerosis and stroke. *Biochimica et biophysica acta*,
1081 doi:10.1016/j.bbadis.2015.10.018 (2015).
1082 104 Argaw, A. T. *et al.* Astrocyte-derived VEGF-A drives blood-brain barrier disruption in
1083 CNS inflammatory disease. *J Clin Invest* **122**, 2454-2468, doi:10.1172/jci60842 (2012).
1084 105 Vanlandewijck, M., Lebouvier, T., Mäe, M. A., Nahar, K. & Betsholtz, C. Primary
1085 isolation of vascular cells from murine brain for single cell sequencing. (2018).
1086 106 Yuan, J. & Sims, P. A. An Automated Microwell Platform for Large-Scale Single Cell
1087 RNA-Seq. *Sci Rep* **6**, 33883, doi:10.1038/srep33883 (2016).

1088 107 Yuan, J. *et al.* Single-cell transcriptome analysis of lineage diversity in high-grade glioma.
1089 *Genome Med* **10**, 57, doi:10.1186/s13073-018-0567-9 (2018).
1090 108 Menon, V. Clustering single cells: a review of approaches on high-and low-depth single-
1091 cell RNA-seq data. *Brief Funct Genomics* **17**, 240-245, doi:10.1093/bfgp/elx044 (2018).
1092 109 Tasic, B. *et al.* Adult mouse cortical cell taxonomy revealed by single cell transcriptomics.
1093 *Nat Neurosci* **19**, 335-346, doi:10.1038/nn.4216 (2016).
1094 110 Sorensen, S. A. *et al.* Correlated gene expression and target specificity demonstrate
1095 excitatory projection neuron diversity. *Cereb Cortex* **25**, 433-449,
1096 doi:10.1093/cercor/bht243 (2015).
1097 111 Hawrylycz, M. *et al.* Canonical genetic signatures of the adult human brain. *Nat Neurosci*
1098 **18**, 1832-1844, doi:10.1038/nn.4171 (2015).
1099 112 Mazzoni, J. *et al.* The Wnt Inhibitor Apcdd1 Coordinates Vascular Remodeling and Barrier
1100 Maturation of Retinal Blood Vessels. *Neuron* **96**, 1055-1069 e1056,
1101 doi:10.1016/j.neuron.2017.10.025 (2017).
1102

1103

1104 **FIGURES AND FIGURE LEGENDS**

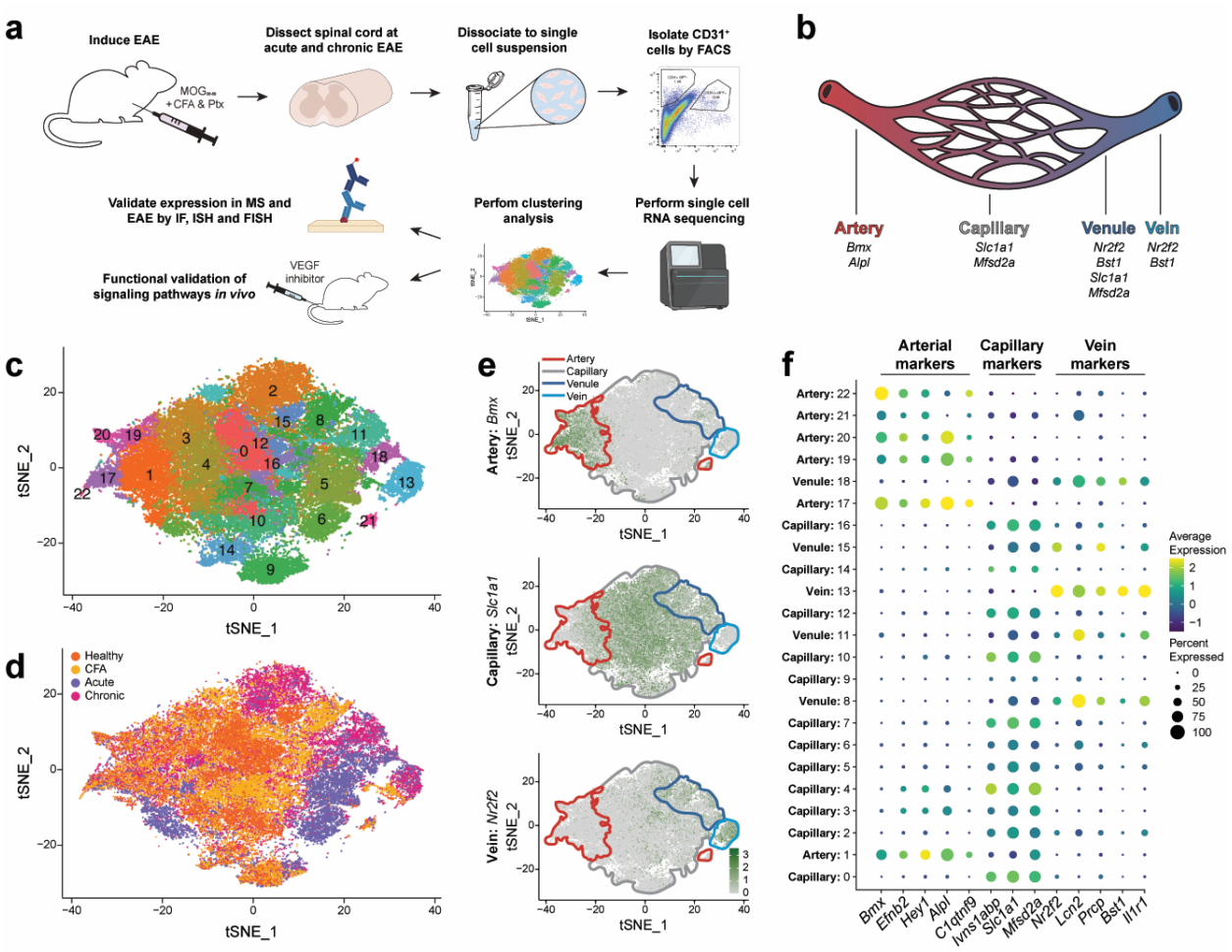

1105

1106

1107 **Figure 1. Single-cell RNA-sequencing and analysis of spinal cord endothelial cells from**
1108 **control and MOG$_{35\text{-}55}$ EAE mice reveals clustering driven by zonation followed by**
1109 **disease/healthy state. a**) Schematic diagram of the experimental workflow for the isolation and
1110 transcriptomic profiling of endothelial cells (ECs) from either healthy (orange), CFA (yellow),
1111 acute (blue) or chronic (magenta) MOG$_{35\text{-}55}$ experimental autoimmune encephalomyelitis (EAE).
1112 We used two mice per sample to obtain sufficient ECs from spinal cords for scRNA-seq analysis.
1113 **b**) Architecture of the mammalian vascular system depicting arteries, capillaries, venules and veins
1114 and some of their specific molecular markers. **c**) t-SNE visualization of the 23 distinct EC clusters
1115 within the scRNA-seq dataset. **d**) t-SNE plot color-coded by sample condition. ECs from acute (n
1116 = 4 samples; blue) and chronic (n = 4 samples; magenta) EAE samples cluster separately from
1117 control ECs [healthy (n = 3 samples; orange) and CFA (n = 3 samples; yellow)], suggestive of

1118 transcriptional shifts in ECs from both acute and chronic EAE. **e**) Feature plots show the
1119 distribution of arterial (*Bmx*), capillary (*Slc1a1*), and venous (*Nr2f2*) marker expression within the
1120 t-SNE plot. Expression of arterial and venous markers peaks at the opposite ends of the t-SNE plot
1121 separated by the capillary marker expression in the middle indicative that zonation is an important
1122 axis of variation among the cells. **f**) Dot plot illustrating the expression of several arterial-,
1123 capillary-, and venous-specific markers within the 23 EC clusters in the scRNAseq dataset.
1124 Clusters are annotated based on marker gene expression.
1125

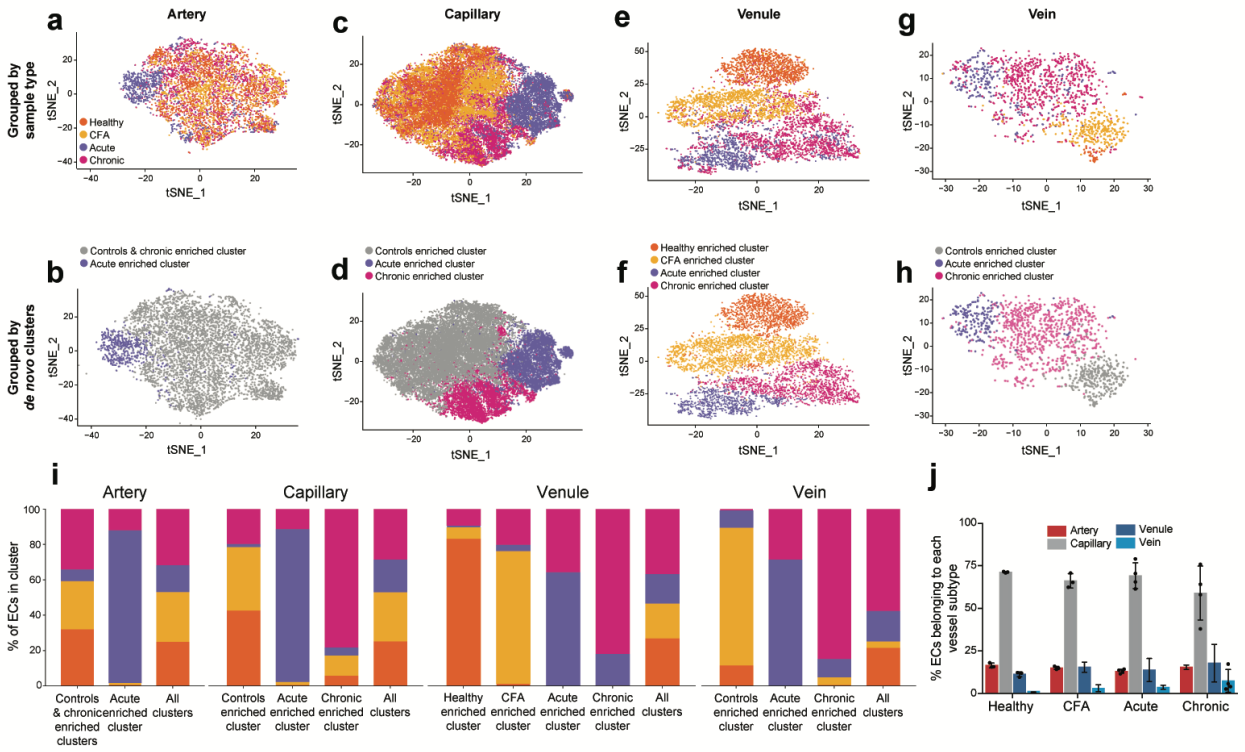

Figure 2. Endothelial subtype-specific t-SNE plots for spinal cords ECs isolated from control and EAE mice show separation of capillary and venous ECs in acute and chronic EAE from the healthy/CFA state. a, c, e, g) Individual t-SNE plots for arterial (aECs; a), capillary (cECs; c), venule (vnECs; e) and vein ECs (vECs; g) color-coded for sample type. **b, d, f, h**) Individual t-SNE plots for aECs (b), cECs (e), vnECs (h) and vECs (k), respectively, depict the clustering of *de novo* clusters for each vessel subtype. There is no clear separation in either the clustering or the t-SNE visualization between the two controls (healthy and CFA) and chronic EAE in aECs (colored in gray) and the two controls (healthy and CFA) in cECs and vECs (colored in gray). **i**) Stacked plots showing the percentage of ECs from each sample type (healthy, CFA, acute or chronic EAE) within the aECs (c), cECs (f), vnECs (i) and vECs (l) t-SNE plots, respectively. j) Dotted bar graphs show the proportion of arterial (aECs; red), capillary (cECs; gray), venule (vnECs; dark blue) and vein (vECs; light blue) ECs isolated from each sample type (healthy, CFA, acute and chronic EAE). Graphs represent mean ± SEM; *$p < 0.05$, **$p < 0.01$, **$p < 0.001$, ****$p < 0.0001$; one-way ANOVA with Tukey test.

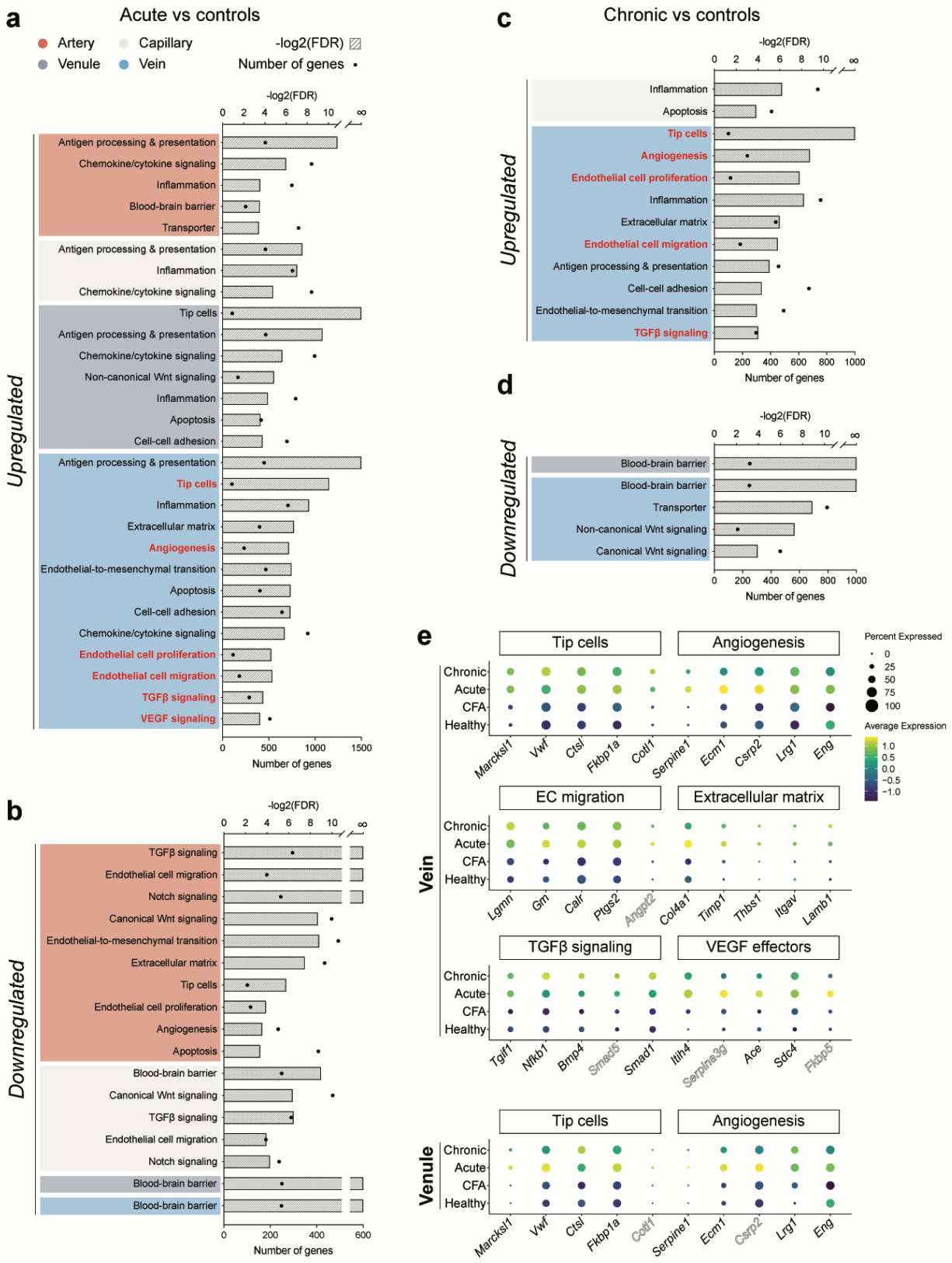
a
Acute vs controls
Artery
Capillary
Venule
Vein
-log2(FDR)
Number of genes
Upregulated
Antigen processing & presentation
Chemokine/cytokine signaling
Inflammation
Blood-brain barrier
Transporter
Antigen processing & presentation
Inflammation
Chemokine/cytokine signaling
Tip cells
Antigen processing & presentation
Chemokine/cytokine signaling
Non-canonical Wnt signaling
Inflammation
Apoptosis
Cell-cell adhesion
Antigen processing & presentation
Tip cells
Inflammation
Extracellular matrix
Angiogenesis
Endothelial-to-mesenchymal transition
Apoptosis
Cell-cell adhesion
Chemokine/cytokine signaling
Endothelial cell proliferation
Endothelial cell migration
TGFβ signaling
VEGF signaling
b
Downregulated
TGFβ signaling
Endothelial cell migration
Notch signaling
Canonical Wnt signaling
Endothelial-to-mesenchymal transition
Extracellular matrix
Tip cells
Endothelial cell proliferation
Angiogenesis
Apoptosis
Blood-brain barrier
Canonical Wnt signaling
TGFβ signaling
Endothelial cell migration
Notch signaling
Blood-brain barrier
Blood-brain barrier
c
Chronic vs controls
Upregulated
Inflammation
Apoptosis
Tip cells
Angiogenesis
Endothelial cell proliferation
Inflammation
Extracellular matrix
Endothelial cell migration
Antigen processing & presentation
Cell-cell adhesion
Endothelial-to-mesenchymal transition
TGFβ signaling
d
Downregulated
Blood-brain barrier
Blood-brain barrier
Transporter
Non-canonical Wnt signaling
Canonical Wnt signaling
e
Vein
Venule
Chronic
Acute
CFA
Healthy
Tip cells
Angiogenesis
EC migration
Extracellular matrix
TGFβ signaling
VEGF effectors
Marcksl1
Vwf
Ctsl
Fkbp1a
Col1l1
Serpine1
Ecm1
Csrp2
Lrg1
Eng
Lgmn
Gm
Calr
Ptgs2
Angpt2
Col4a1
Timp1
Thbs1
Itgav
Lamb1
Tgfi1
Nfkb1
Bmp4
Smad5
Smad1
Itih4
Serpine3g
Ace
Sdc4
Fkbp5
Percent Expressed
0
25
50
75
100
Average Expression
1.0
0.5
0.0
−0.5
−1.0

1143

1144 **Figure 3. Gene set enrichment analysis (GSEA) reveals that transcriptome signatures of neo-**
1145 **angiogenesis are present in vein ECs from both acute and chronic EAE. a, c**)
1146 Pathways/processes upregulated in diseased arterial (red), capillary (light gray), venule (dark
1147 blue), and venous (light blue) ECs in acute (a; 16 d.p.i) and chronic (c, 28 d.p.i) EAE versus
1148 controls. The gene ontology enrichment plots, derived using the GSEA algorithm, indicate that
1149 gene sets related to neo-angiogenesis (highlighted in red) are significantly upregulated in diseased
1150 vECs, and to a lesser extent, vnECs, relative to controls, in both acute and chronic EAE. **b, d**)
1151 Pathways/processes significantly downregulated in diseased arterial (red), capillary (gray), venule
1152 (venetian blue) and venous (pool blue) ECs in acute (b), and chronic (d), EAE versus controls.
1153 Expression of the blood-brain barrier gene set is significantly reduced in diseased ECs of all vessel
1154 subtypes, except arteries. **e**) Dot plots for expression of angiogenesis, tip cells, EC migration,
1155 extracellular matrix, VEGF and TGF-β pathway genes in vECs show increased average expression
1156 in both acute and chronic EAE. vnECs also upregulate expression of tip cell markers in acute and
1157 chronic EAE. Genes presented in solid typeface significantly upregulate during both acute and
1158 chronic EAE stages, whereas those in outlined font (Angpt2, Smad5, Serpina3g, Fkbp5, Cotl1, and
1159 Csrp2) show marked upregulation solely in the acute EAE phase.
1160

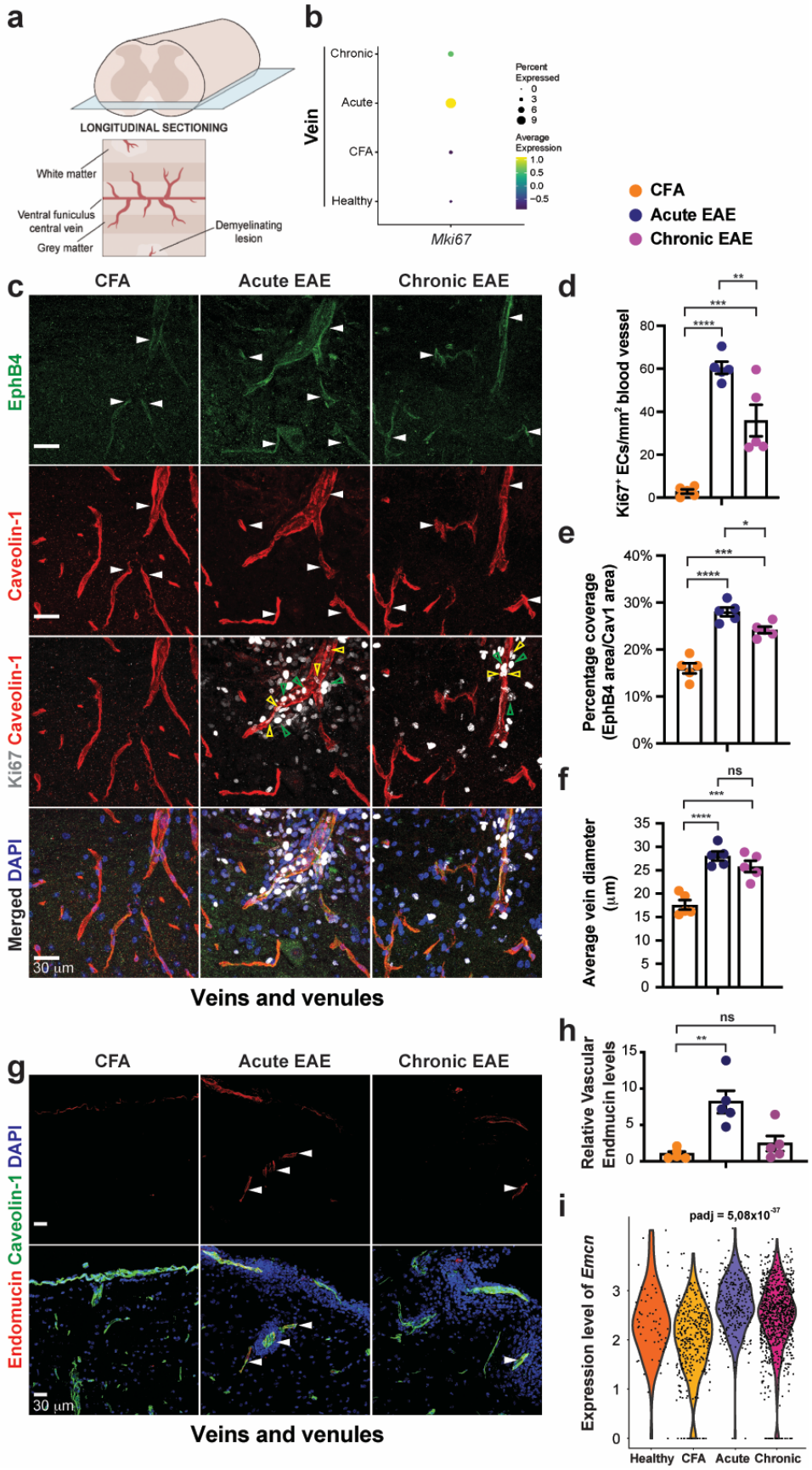
a
LONGITUDINAL SECTIONING
White matter
Ventral funiculus central vein
Grey matter
Demyelinating lesion
b
Chronic
Acute
CFA
Healthy
Vein
Mki67
Percent Expressed
Average Expression
CFA
Acute EAE
Chronic EAE
c
CFA
Acute EAE
Chronic EAE
EphB4
Caveolin-1
Ki67 Caveolin-1
Merged DAPI
30 µm
Veins and venules
d
Ki67+ ECs/mm2 blood vessel
e
Percentage coverage (EphB4 area/Cav1 area)
f
Average vein diameter (µm)
ns
h
Relative Vascular Endmucin levels
g
CFA
Acute EAE
Chronic EAE
Endomucin Caveolin-1 DAPI
30 µm
Veins and venules
i
padj = 5,08x10-37
Expression level of Emcn
Healthy
CFA
Acute
Chronic

1161

1162 **Figure 4. Increased vein EC proliferation in EAE leads to enlarged veins and higher venous**
1163 **coverage. a)** Schematic diagram of the spinal cord longitudinal (sagittal) sections used throughout
1164 the study to measure *in vivo* protein/mRNA expression in control and EAE. **b)** Dot plot generated
1165 from the scRNA-seq dataset shows that *Mki67* mRNA expression is upregulated in acute, and to a
1166 lesser extent chronic, vECs. **c)** Sagittal sections of control (CFA), acute (16 d.p.i) and chronic (28
1167 d.p.i) EAE spinal cords were immunostained with antibodies against EphB4 (venous ECs) and
1168 Ki67 (proliferation) along with Caveolin-1 (EC marker) and DAPI. White arrowheads point at
1169 EphB4^{+}/Caveolin-1^{+} (double positive) vessels. Empty yellow arrowheads point at Ki67^{+} ECs.
1170 Empty green arrowheads point at Ki67^{+} immune cells. **d, e, f)** Dotted bar graphs showing
1171 quantification of number of Ki67^{+} ECs in EphB4^{+} vessels (d), EphB4^{+} vascular area (e) and vein
1172 diameter (f) reveal significantly higher EC proliferation, venous coverage and vein diameter in
1173 acute and chronic EAE spinal cords compared to the control (n = 5). **g)** Sagittal sections of control
1174 (CFA), acute EAE and chronic EAE spinal cords were immunostained for Endomucin (marks
1175 venous ECs), combined with immunostaining for Caveolin-1 (EC marker) and DAPI. White
1176 arrowheads point at expression of Endomucin in blood vessels. **h)** Dotted bar graphs showing
1177 relative expression level of Endomucin reveal significantly higher expression level in acute EAE
1178 spinal cord ECs compared to the control (n = 5). **i)** Violin plots for *Emcn* mRNA expression in
1179 control (healthy and CFA), acute and chronic EAE vECs generated from the scRNA-seq dataset.
1180 Graphs represent mean ± SEM from n = 5 mice/group; *$p < 0.05$, **$p < 0.01$, **$p < 0.001$, ****p
1181 < 0.0001; one-way ANOVA with Tukey test. Scale bars = 30 μm.
1182

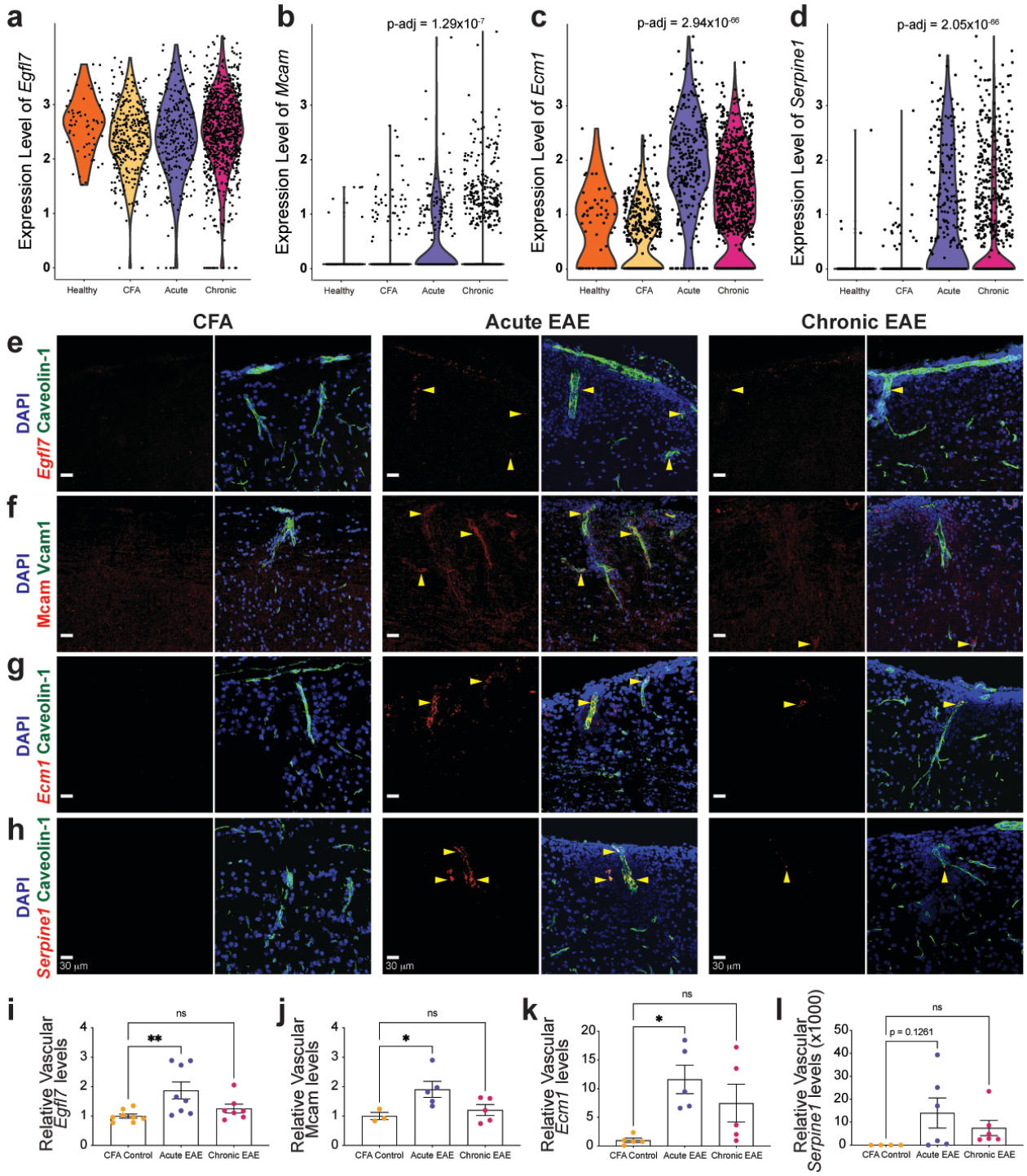

Figure 5. Expression of several tip cell/angiogenesis markers are upregulated by ECs in acute EAE. a-d) Violin plots for *Egfl7*, *Mcam*, *Ecm1* and *Serpine1* mRNA expression in control (healthy and CFA), acute and chronic EAE vECs generated from the scRNAseq dataset. e, f, g, h) Sagittal sections of control (CFA), acute and chronic EAE spinal cords were probed with fluorescence *in*

1189 *situ* hybridization (FISH) for *Egfl7* (e), *Ecm1* (g) and *Serpine1* (h) mRNAs or immunostained for
1190 Mcam (f), combined with immunostaining for Caveolin-1 (EC marker) or Vcam1 (venous marker)
1191 and DAPI. Yellow arrowheads point at the expression of corresponding markers in blood vessels.
1192 i, j, k, l) Dotted bar graphs showing relative expression levels of *Egfl7* (i), Mcam (j), *Ecm1* (k) and
1193 *Serpine1* (l) reveal significantly higher expression levels in acute EAE spinal cord ECs compared
1194 to the control. Data represent mean ± SEM; *$p < 0.05$, **$p < 0.01$, ****$p < 0.0001$; one-way
1195 ANOVA with Bonferroni's multiple comparisons test. Scale bars = 30 μm.
1196

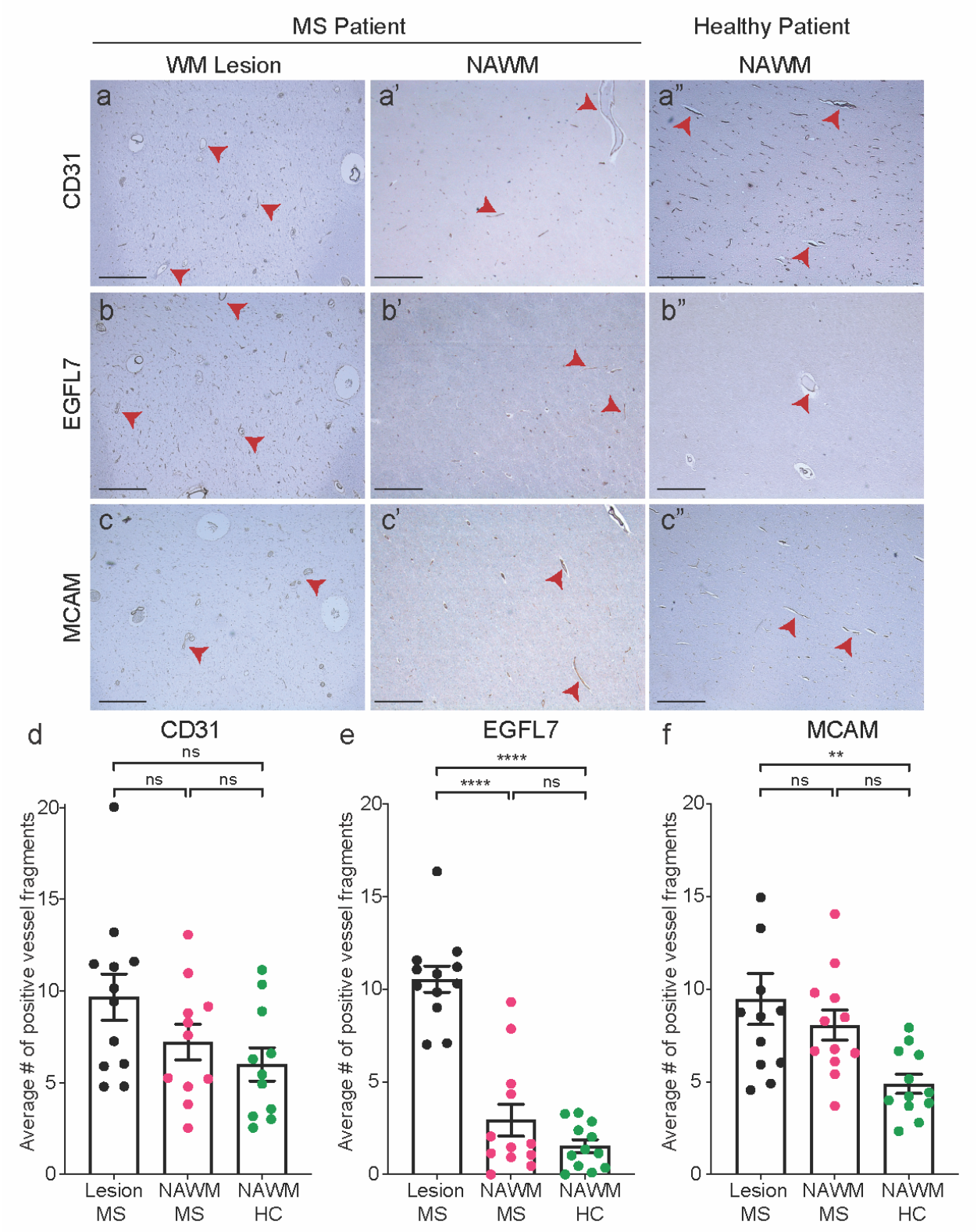
MS Patient
Healthy Patient
WM Lesion
NAWM
NAWM
CD31
EGFL7
MCAM
a
a'
a"
b
b'
b"
c
c'
c"
d
CD31
e
EGFL7
f
MCAM
ns
ns
ns
****
****
ns
**
ns
ns
Average # of positive vessel fragments
0
5
10
15
20
Lesion MS
NAWM MS
NAWM HC

1197

1198

1199 **Figure 6. Increased expression of angiogenic markers in human multiple sclerosis lesions. a,**
1200 **a', a''**) Immunohistochemistry (IHC) staining for CD31 (EC marker) in white matter (WM) lesions
1201 of MS patients (a), normal appearing white matter (NAWM) of an MS patient (a') or a non-
1202 neurological control case (a''). **b, b', b''**) IHC for the angiogenic marker, EGFL7, shows increased
1203 expression in WM lesions of MS patients (b) relative to NAWM of both the MS (b') and a non-
1204 neurological control case (b''). **c, c', c''**) IHC for the angiogenic marker, MCAM, shows increased
1205 expression in WM lesions of MS cases (c), relative to NAWM of non-neurological control case
1206 (c''). **b-c''**) Hematoxylin was used as a nuclear counterstain. **d, e, f**) Dotted bar graphs of the $CD31^+$
1207 average vessel density per given area (d), average EGFL7 (e), and MCAM (f) expression in blood
1208 vessels located in WM lesions and NAWM of MS patients (N = 11-12) and NAWM of non-
1209 neurological control patients (N = 11-12). Data represent mean ± SEM; n.s. = non-significant, *p
1210 < 0.05, **p < 0.01, ****p < 0.0001; two-tailed Student's t test. Scale bars = 200 μm.
1211

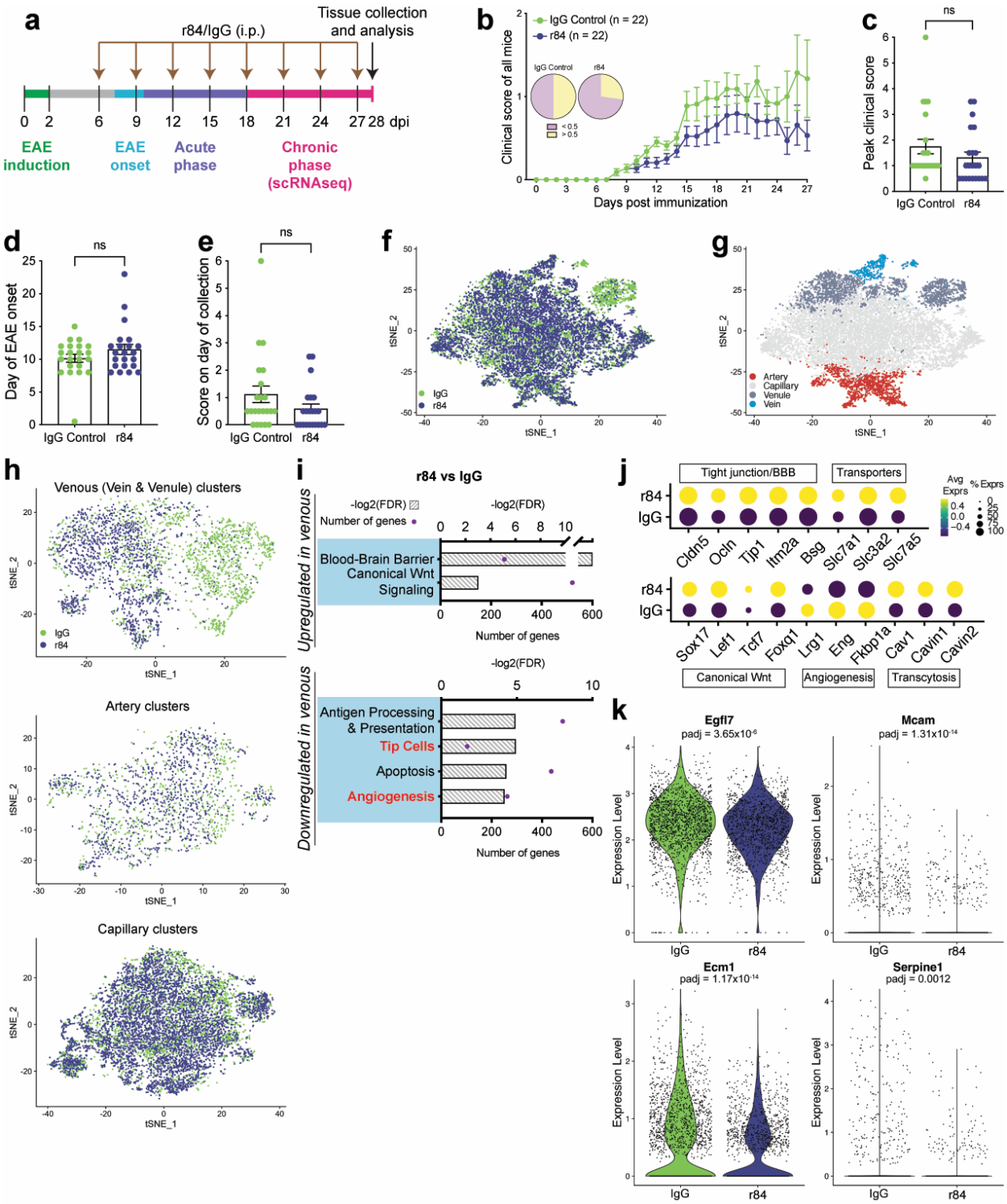

Figure 7. Gene set enrichment analysis (GSEA) reveals that transcriptome signatures of neo-angiogenesis are downregulated in spinal cord ECs of chronic EAE mice following treatment with r84. a) Diagram of the experimental procedure. Following EAE induction, mice were

1217 injected intraperitoneally (i. p.) every 3 days with either 5 mg/kg anti-VEGF monoclonal antibody
1218 r84, or an isotype control immunoglobulin G1 (IgG1), from 6 until 27 d.p.i. (chronic phase). Tissue
1219 was collected at 28 d.p.i. for analyses. **b**) Clinical EAE score curves for r84- and IgG1-treated
1220 mice. The inset pie charts depict the fraction of mice with clinical scores < 0.5 (pink) and > 0.5
1221 (yellow) in the two treatment groups. The IgG1-treated EAE mice exhibit higher incidence of
1222 clinical scores > 0.5 compared to r84-treated EAE mice. **c-e**) Dotted bar graphs show no significant
1223 difference between the peak clinical score (c), day of disease onset (d), and score on the day of
1224 collection (e) between two groups. **f**) t-SNE visualization of ECs isolated from r84-treated (n = 3
1225 samples; 6 mice) and IgG-treated (n = 3 samples; 8 mice) EAE spinal cords, color-coded for
1226 treatment. **g**) t-SNE plot, color-coded for EC subtype, shows that r84- and IgG treated ECs in this
1227 representation are visually organized along the arteriovenous zonation gradient. **h)** t-SNE plots,
1228 color coded for treatment, showing clustering of venous (vein & venule), arterial and capillary ECs
1229 in r84- and IgG-treated EAE mice. Only venous (vein & venule) ECs have non-overlapping
1230 clusters for r84 and IgG treatment groups. **i**) Pathways/processes significantly up- and
1231 downregulated in r84-treated relative to IgG-treated chronic (28 d.p.i) EAE venous (vein & venule)
1232 ECs. The gene ontology enrichment plots, derived using the GSEA algorithm, show that
1233 expression of neo-angiogenic gene sets and pathways (highlighted in red) are significantly
1234 downregulated in r84 EAE ECs. **j**) Dot plot shows significant upregulation of tight junction/BBB,
1235 transporter, canonical Wnt and transcytotic genes, and significant downregulation of angiogenic
1236 genes, in r84-treated venous (vein & venule) chronic (28 d.p.i) EAE ECs. **k**) Violin plots depicting
1237 reduction in *Egfl7*, *Mcam*, *Ecm1* and *Serpine1* expression levels in r84- relative to IgG-treated
1238 chronic (28 d.p.i) EAE venous (vein & venule) ECs. Data represent mean ± SEM; * $p < 0.05$, ** p
1239 < 0.01, **** $p < 0.0001$; b) one-way ANOVA with repeated measures; c, d, e) two-tailed Student's
1240 t-test.
1241

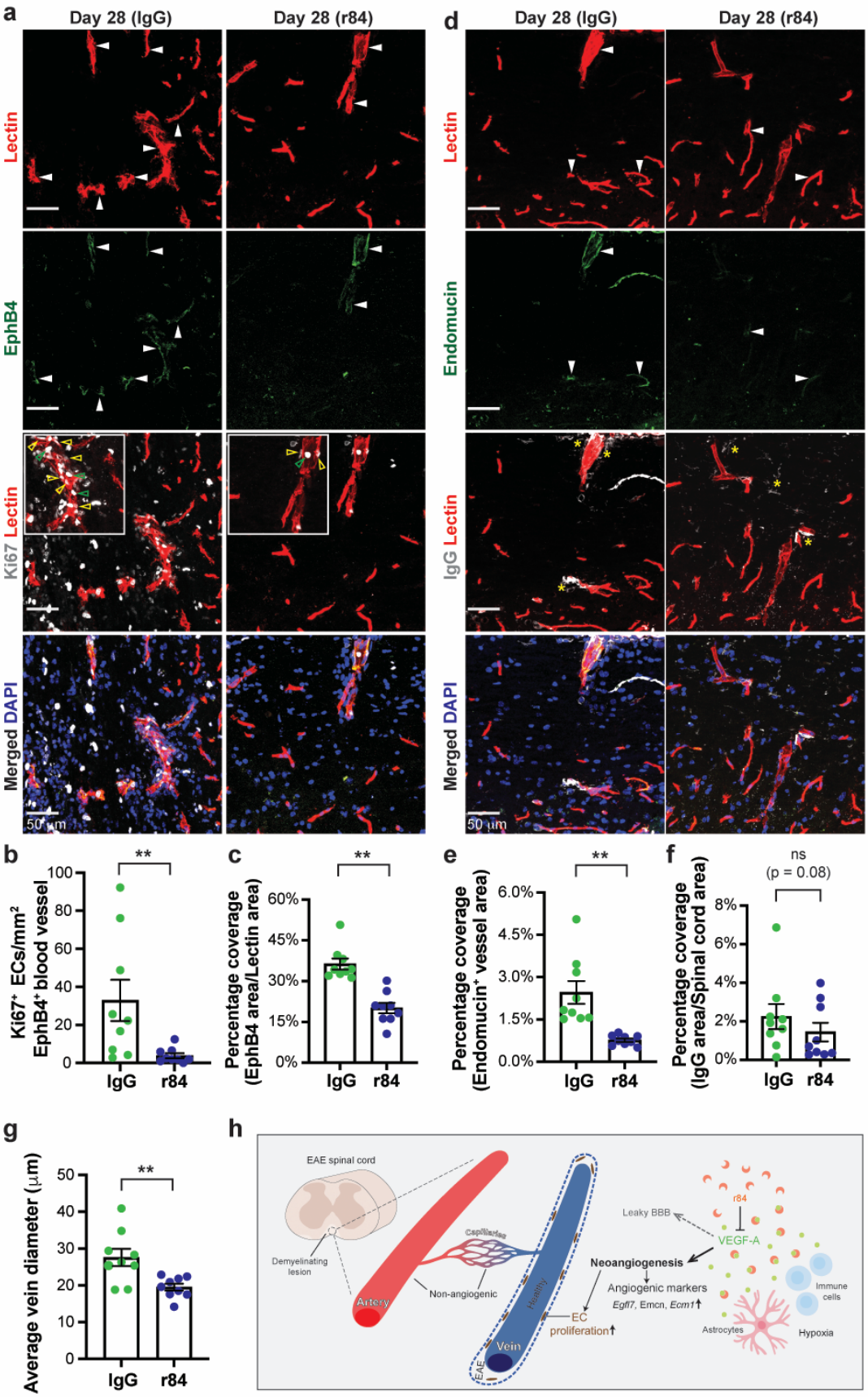
a
Day 28 (IgG)
Day 28 (r84)
Lectin
EphB4
Ki67 Lectin
Merged DAPI
50 µm
d
Day 28 (IgG)
Day 28 (r84)
Lectin
Endomucin
IgG Lectin
Merged DAPI
50 µm
b
Ki67+ ECs/mm2 EphB4+ blood vessel
IgG
r84
c
Percentage coverage (EphB4 area/Lectin area)
IgG
r84
e
Percentage coverage (Endomucin+ vessel area)
IgG
r84
f
Percentage coverage (IgG area/Spinal cord area)
ns
(p = 0.08)
IgG
r84
g
Average vein diameter (µm)
IgG
r84
h
EAE spinal cord
Demyelinating lesion
Capillaries
Non-angiogenic
Artery
Vein
Healthy
EAE
EC proliferation↑
Leaky BBB
r84
VEGF-A
Neoangiogenesis
Angiogenic markers
Egfl7, Emcn, Ecm1↑
Immune cells
Astrocytes
Hypoxia

1242

1243 **Figure 8. r84 treatment reduces pathological neo-angiogenesis in vein ECs in EAE, but does**
1244 **not rescue BBB leakage. a)** Sagittal sections of IgG- and r84-treated 28 d.p.i. EAE spinal cords
1245 were immunostained with antibodies against EphB4, Ki67 as well as DAPI following cardiac
1246 perfusion with Lectin (marks perfused ECs). White arrowheads point at EphB4$^+$/Lectin$^+$ (double
1247 positive) vessels. Empty yellow arrowheads point at Ki67$^+$ ECs. Empty green arrowheads point at
1248 Ki67$^+$ immune cells. **b, c)** Dotted bar graphs of the number of Ki67$^+$ ECs in EphB4+ vessels (b)
1249 and EphB4$^+$ vascular area (c) show lower EC proliferation and venous coverage in r84-treated
1250 spinal cords compared to the control (n = 9 mice /group). **d)** Sagittal sections of IgG- and r84-
1251 treated 28 d.p.i. EAE spinal cords were immunostained with antibodies against Endomucin (marks
1252 veins), endogenous serum IgG and DAPI after cardiac perfusion with Lectin. White arrowheads
1253 point at Endomucin$^+$/Lectin$^+$ (double positive) vessels. Yellow asterisks point at serum IgG
1254 leakage around blood vessels. **e-f**) Dotted bar graphs show quantification of Endomucin$^+$ vascular
1255 area (e) and IgG leakage area (f). There was significantly lower venous coverage but no significant
1256 difference in IgG leakage area in r84-treated spinal cords compared to the control (n = 9 mice /
1257 group). **g)** Dotted bar graph showing quantification venous diameter reveals significant reduction
1258 in r84-treated spinal cords compared to the control (n = 9 mice / group). **h)** Model illustrating the
1259 putative mechanism of pathological neo-angiogenesis in EAE. Neuroinflammation induces
1260 enlargement of veins and venules (via vEC proliferation), with leaky BBB, via neo-angiogenesis
1261 in the white matter lesions of the spinal cord, where there is a significant presence of infiltrating
1262 immune cells. Hypoxic conditions induce secretion of VEGF-A from either infiltrating immune
1263 cells (e.g. macrophages), or CNS resident cells (e.g. astrocytes), resulting in activation of VEGF-
1264 A signaling pathway in vECs. Blockade of VEGF-A signaling through administration of r84
1265 reduces neo-angiogenesis. But r84 treatment does not reduce disease severity, immune cell
1266 infiltration and BBB permeability. Our study identifies VEGF-A signaling as a driver of neo-
1267 angiogenesis in neuroinflammation.